LLNL-JRNL-672059

LAWRENCE
LIVERMORE
NATIONAL
LABORATORY

Methods of Photoelectrode Characterization with High Spatial and Temporal Resolution

D. V. Esposito, J. B. Baxter, J. John, N. S. Lewis, T. P. Moffat, T. Ogitsu, G. D. O'Neil, T. A. Pham, A. A. Talin, J. M. Velazquez, B. C. Wood

June 3, 2015

Energy & Environmental Science

Disclaimer

This document was prepared as an account of work sponsored by an agency of the United States government. Neither the United States government nor Lawrence Livermore National Security, LLC, nor any of their employees makes any warranty, expressed or implied, or assumes any legal liability or responsibility for the accuracy, completeness, or usefulness of any information, apparatus, product, or process disclosed, or represents that its use would not infringe privately owned rights. Reference herein to any specific commercial product, process, or service by trade name, trademark, manufacturer, or otherwise does not necessarily constitute or imply its endorsement, recommendation, or favoring by the United States government or Lawrence Livermore National Security, LLC. The views and opinions of authors expressed herein do not necessarily state or reflect those of the United States government or Lawrence Livermore National Security, LLC, and shall not be used for advertising or product endorsement purposes.

Submitted to: Energy & Environmental Science

Article Type: Review

Methods of Photoelectrode Characterization with High Spatial and Temporal Resolution

Daniel V. Esposito,[1,2*] Jason B. Baxter,[3] Jimmy John,[4] Nathan S. Lewis,[4] Thomas P. Moffat,[2]
Tadashi Ogitsu,[6] Glen D. O'Neil,[1] Tuan Anh Pham,[6] A. Alec Talin,[5] Jesus M.Velazquez,[4]
Brandon C. Wood[6]

[1] Columbia University

[2] National Institute of Standards and Technology

[3] Drexel University

[4] Joint Center for Artificial Photosynthesis, California Institute of Technology

[5] Sandia National Laboratories

[6] Lawrence Livermore National Laboratory

*Corresponding Author

Daniel V. Esposito

de2300@columbia.edu

Ph: 212-854-2648

Abstract

Materials and photoelectrode architectures that are highly efficient, extremely stable, and made from low cost materials are required for commercially viable photoelectrochemical (PEC) water-splitting technology. A key challenge is the heterogeneous nature of real-world materials, which often possess spatial variation in their crystal structure, morphology, and/or composition at the nano-, micro-, or macro-scale. Different structures and compositions can have vastly different properties and can therefore strongly influence the overall performance of the photoelectrode through complex structure-property relationships. A complete understanding of photoelectrode materials would also involve elucidation of processes such as carrier collection and electrochemical charge transfer that occur at very fast time scales. We present herein an overview of a broad suite of experimental and computational tools that can be used to define the structure-property relationships of photoelectrode materials at small dimensions and on fast time scales. A major focus is on *in situ* scanning-probe measurement (SPM) techniques that possess the ability to measure differences in optical, electronic, catalytic, and physical properties with nano- or micro-scale spatial resolution. *In situ* ultrafast spectroscopic techniques, used to probe carrier dynamics involved with processes such as carrier generation, recombination, and interfacial charge transport, are also discussed. Complementing all of these experimental techniques are computational atomistic modeling tools, which can be invaluable for interpreting experimental results, aiding in materials discovery, and interrogating PEC processes at length and time scales not currently accessible by experiment. In addition to reviewing the basic capabilities of these experimental and computational techniques, we highlight key opportunities and limitations of applying these tools for the development of PEC materials.

Key Words: photoelectrochemical cells, photoelectrodes, solar fuels, water splitting, scanning-probe microscopy, ultrafast spectroscopy, computational modeling, first-principles modeling, in situ experiments, nanoscale, microscale, materials development, scanning-photocurrent spectroscopy, scanning-electrochemical microscopy, scanning-tunneling microscopy, spectroelectrochemistry, Raman spectroscopy

1. Introduction

The generation of hydrogen through photoelectrochemical (PEC) water splitting, whereby light is used to electrochemically split water into molecular hydrogen and oxygen, is a promising approach to producing storable, scalable, and carbon-free renewable energy.[1–4] However, no PEC system has been demonstrated to date that can meet the efficiency, stability, and cost targets[5] needed for an economically viable PEC technology.[6] One of the major barriers to commercialization is the lack of suitable materials to be used in photoelectrodes,[2,4] the "engines" of PEC devices that are responsible for absorbing light and using the resulting potential energy difference to drive the water splitting reaction. To perform these functions with high efficiency and durability, photoelectrode materials and architectures are needed that are extremely stable, absorb a significant portion of the solar spectrum, possess high catalytic activity for the hydrogen- and oxygen-evolution reactions (HER and OER, respectively), produce a large photovoltage, exhibit high carrier lifetimes, and are predominantly comprised of earth-abundant elements.

Finding a single material or combination of materials that are capable of meeting all of these requirements is a daunting task. Ever since Fujishima and Honda first demonstrated PEC water splitting with TiO_2 in 1973,[7] many different classes of semiconductors have been explored as photoelectrode absorbers, including metal oxides, chalcopyrites, chalcogenides, group III-V semiconductors, group V semiconductors (Si), and more.[3,8–10] None of these materials, by themselves, are capable of meeting all of the aforementioned photoelectrode requirements. However, the opportunity to discover a suitable photoelectrode material or combination of materials is tremendous when one considers that there are ≈800 two-component and $\approx 10^4$ tri-component combinations of earth-abundant elements,[11] and a nearly infinite number of atomic arrangements. The use of composite photoelectrode architectures containing a combination of semiconducting absorber(s), metallic catalysts, and protective insulating layers increases the number of compositional permutations even further.

Due to the sheer number of candidate materials, high-throughput experimental[12–16] and computational[17,18] screening methods naturally lend themselves as useful tools for *identifying* promising photoelectrode materials. However, the *development* process only begins once a new, promising material composition has been identified. Subsequently, realizing the full potential of a material for PEC water splitting requires rigorous downstream optimization and experimentation. Through different synthesis methods and conditions, many parameters can be varied to optimize a material's performance, including crystal phases and orientations, composition, morphology, substrate and co-catalyst selection, dopant distribution, defect engineering, and more. All of these factors can have a huge impact on the overall performance of a photoelectrode. Unfortunately, precise and independent control of these factors is generally not possible. For example, many materials are highly heterogeneous in nature, possessing variation in crystallinity, composition, and/or morphology at the nano-, micro-, and/or macro-scales. Heterogeneous photoelectrodes often result in macro-scale performance that is a complex convolution of the local performance associated with different compositions, structures, and morphologies. Additionally, most fundamental processes involved with PEC energy conversion are dynamic processes taking place over timescales typically ranging from femtoseconds (fs) to microseconds (μs).[19]

Deconvolving the structure-property relationships *in situ* with high spatial and temporal resolution is thus important for obtaining an advanced understanding of photoelectrode behavior and then using that knowledge to design better photoelectrodes. The study of photoelectrodes *in situ* and under real or simulated operating conditions in an electrochemical environment is especially important because the properties and characteristics of a photoelectrode are often intimately coupled to the properties of the liquid-phase electrolyte.[20,21] For example, the electrolyte can strongly affect the chemical and electronic properties of the surface and space-charge layer of the photoelectrode, and therefore influence catalytic, charge transport, and corrosion processes. *Ex situ* techniques performed in atmosphere or vacuum can also provide important and complementary information about a photoelectrode material, but cannot substitute for viewing the true physical and chemical state of the material in a photoelectrochemical environment. Fortunately, many experimental and computational tools are well-suited for the measurement of spatially varying properties and/or ultrafast carrier dynamics in a PEC environment. Table I lists the major types of experimental techniques that are suitable for *in situ* analysis of photoelectrodes with high spatial and/or temporal resolution. Table II, to be discussed in Section 4, provides similar information for atomistic computational tools.

Table I can be split into two broad types of techniques: scanning probe measurement (SPM) techniques used for achieving high spatial resolution, and pump-probe type spectroscopic techniques used for monitoring ultrafast processes with high temporal resolution. Several major uses and benefits of *in situ* techniques with high spatial and/or temporal resolution are as follows:

i. ***Diagnostic-*** By investigating the spatial variation in properties or performance of a photoelectrode, SPM techniques can be used to locate poorly performing “cold spots” and highly performing “hot spots” on the photoelectrode. Using additional *in situ* or *ex situ* characterization, the structural and/or compositional variation that gives rise to the regions of anomalous performance can then be identified. Likewise, fast events like charge-carrier recombination and interfacial charge transfer can be studied to complement SPM techniques by identifying rate-limiting processes. This information can be an important source of feedback for optimization of the design of the photoelectrode.

ii. ***Mechanistic-*** Carefully-designed SPM and/or ultrafast spectroscopy measurements can provide a deeper understanding of physical, opto-electronic, and catalytic PEC processes, allowing for further refinement of the computational models used for identifying even better photoelectrode materials

iii. ***Screening-*** Many *in situ* SPM techniques are well suited for rapid measurement of the properties or performance of large arrays of (typically) millimeter-sized samples for the purpose of high-throughput screening. Generally, high spatial resolution and ultrafast spectroscopy are not needed in these studies, and the reader is referred to other literature on the topic.[12,15,16,22–27]

The remainder of this paper provides an overview of *in situ* SPM techniques (Section 2), ultrafast spectroscopy techniques (Section 3), and computational tools (Section 4) that have been used, or have the potential to be used, for *in situ* investigation photoelectrodes with high spatial and/or temporal resolution. In addition to describing the basic principles behind each class of techniques, the opportunities and challenges for using these methods for *in situ* studies are discussed. In Section 5, two final topics are covered: i.) coordination of advanced SPM and ultrafast measurements with more common macro-scale PEC characterization techniques, and ii.) simultaneous use of multiple *in situ* techniques.

2. *In situ* Techniques for Evaluation of Photoelectrodes with High Spatial Resolution

This section focuses on *in situ* scanning-probe measurement (SPM) techniques, broadly defined as techniques in which a probe is scanned across the surface of a sample while the interaction between the probe and surface is recorded as a function of the position of the probe. Depending on the nature of the probe and its interaction with the surface (optical, electronic, force, magnetic, etc), the properties of the surface can be determined with a spatial resolution that is generally commensurate with the diameter of the probe. For most of the SPM techniques discussed herein, modified or custom-made PEC test cells and samples are often necessary for *in situ* measurements to be performed. Additionally, sample and test cell requirements are often dependent on the specific SPM technique being employed. The following sections provide some basic information about experimental set-ups and procedures, but the reader is directed towards technique-specific references for more detailed descriptions.

2.1 Scanning photocurrent methods

Scanning-photocurrent microscopy (SPCM), also referred to as light-beam-induced current (LBIC) and optical-beam-induced current (OBIC), is a technique in which a scanning optical probe, typically a laser beam, is used to measure the local variation in sample photocurrent or photovoltage as a function of the beam position on the photoelectrode surface. In most SPCM measurements, a laser beam consisting of monochromatic, collimated light with a high degree of coherency is focused to a small spot on the photoelectrode surface. When used to study materials for PEC or PV applications, the wavelength of light emitted from the laser is usually chosen such that the corresponding photon energy is greater than the band gap of the semiconductor, allowing the focused laser beam to *locally* generate electron-hole pairs in the semiconductor. When the photoelectrode is tested under appropriate applied bias, the resulting photocurrent or photovoltage can be measured as a function of laser beam position as the laser or sample position is varied with a nano- or micro-positioning system (Fig. 1a). The raw photocurrent or voltage is valuable information by itself, but the method can also been used to determine spatial variation in quantum yield,[28–30] minority carrier diffusion length,[31,28] electric field distributions,[31] photoconductivity, dopant concentrations,[31] and more.

In PEC systems, the measured photocurrent is strongly dependent on the optical, electronic, and catalytic properties of the photoelectrode. Assessing the relative contributions from these different properties of the photoelectrode surface can be challenging, but is possible through systematic control of the various operational parameters of SPCM, including but not limited to: the applied potential; the wavelength of the optical excitation; the laser intensity; comparison between photovoltage and photocurrent mode; and the type of electrolyte. For example, varying the applied potential strongly effects catalysis and carrier collection in a photoelectrode, but should have minimal influence on the optical properties of most materials.

The best spatial resolution that can be achieved by conventional far-field SPCM techniques is set by the optical diffraction limit, also referred to as the Abbe diffraction limit. This limit states that the smallest possible light beam diameter is given by $d = \lambda/2NA$, where λ is the wavelength of incident light and $NA=n\cdot\sin(\theta)$ is the numerical aperture of the focusing lens.[32–34] The value of NA depends on the aperture angle (θ) of the specific lens and on the index of refraction of surrounding medium (n), with $NA\approx1.5$ being the highest value theoretically possible using an oil immersion, high magnification lens.[34] For visible light wavelengths, the best resolution based on conventional microscope arrangements is typically ≈ 500 nm- 1 μm.[35] To achieve such spatial resolution, short wavelength lasers combined with high NA objectives, often with very small working distances, must be employed.

Due to the optical diffraction limit, spatially resolved SPCM measurements of nano-sized features and phenomena cannot be obtained using conventional SPCM. Fortunately, several optical imaging techniques offer the ability to interrogate samples with resolution better than the Abbe diffraction limit. Far field optical imaging techniques based on photoswitching and saturation of fluorescence have demonstrated resolution less than 30 nm,[36–38] but the optical probe itself is still diffraction limited. Another SPM technique capable of breaking the Abbe diffraction limit is near-field scanning optical microscopy (NSOM),[39,40] in which incident light is typically fed through an optical fiber having an aperture at the tip of the fiber (Figure 1b). Although NSOM is typically used for optical imaging, NSOM probes can also be used for SPCM measurements of photo-active samples. SPCM conducted with an NSOM probe, also known as near field scanning photocurrent microscopy and photoelectrochemical microscopy, has been successfully used to study nanoscale variation in photocurrent in photovoltaic materials,[41–43] and analysis of corrosion products.[44] NSOM-based SPCM offers similar opportunities for investigation of photoelectrodes at the nanoscale range. In conventional NSOM probes, the size of this aperture is crucial for setting the resolution. In an alternate design, nano-scale metallic tips can be used to transform light from the far field to the near field through the use of surface plasmons.[45,46]Although near-field approaches to SPCM such as NSOM possesses the ability to resolve nanoscale features, NSOM also presents several challenges in implementation, including limitations on sensitivity, bandwidth, resolution, compatibility with rough surfaces, and sample/cell geometries. Modifying NSOM tips and tools for the *in situ* SPCM investigation of photoelectrode materials that possess nanoscale features is a challenging but potentially highly rewarding opportunity in the PEC field.

In addition to the challenge of achieving sub-micron spatial resolution, several other limitations are commonly encountered in SPCM, including diffraction-limited spatial resolution; illumination by a non- Air Mass (AM) 1.5 light source; back-reaction under non-uniform illumination; and bubble formation. Researchers must be especially conscientious of the differences between local illumination by an intense, often-polarized, monochromatic light source and a broad spectrum AM 1.5 light source that is commonly used in macro-scale measurements. Even though the net power of a laser beam used for SPCM is usually set very low, the light intensity at the laser spot on the sample surface can be orders of magnitude larger than that obtained using AM 1.5 illumination. Operating a photoelectrode under high light intensities can result in high carrier injection conditions, resulting in substantially different underlying physics for carrier generation, recombination, and collection than under 1-sun intensity.[47] Furthermore, the correspondingly large local photocurrent densities can lead to higher local catalytic overpotentials, significant pH gradients, and the formation of bubbles due to supersaturation of the local electrolyte with the product H_2 or O_2. Performing SPCM in PEC systems therefore necessitates a careful trade-off between signal-to-noise ratio, resolution, and obtaining photocurrent behavior that is consistent with solar illumination. A better quantitative understanding of the trade-offs, aided by computational modeling, would be of great use for advancing the application of SPCM to studying photoelectrode surfaces.

2.2 Scanning Electrochemical Microscopy

We provide here a brief introduction to scanning electrochemical microscopy (SECM), and detailed monographs covering the fundamentals, experimental details, and advanced applications of SECM are available elsewhere.[48–52] In an SECM experiment an ultramicroelectrode (UME) is used as an electrochemical scanning probe. UMEs are typically metallic disks or rings that are embedded in an insulating material (i.e. – glass or wax) and have a critical dimension that is usually less than ≈25 µm.[48] The UME tip is positioned in close proximity to the substrate, typically within two tip radii, where the tip interacts with the substrate via an electrochemically active redox mediator species. When used to study photocathode or photoanode materials for water splitting, the redox mediator species of interest are H^+/H_2 and H_2O/O_2, respectively. As shown in Figure 2 for a H_2-evolving photocathode, one of the most common modes of SECM operation is substrate generation/ tip collection mode, whereby H_2 is generated from the reduction of protons at the photoelectrode while the UME tip oxidizes the H_2 back to H^+. This method is implemented by using a bipotentiostat to independently controlling the potentials of the photoelectrode and UME while measuring the current between them. For photoanodes, H_2O is oxidized at the photoelectrode and O_2 is reduced at the UME. Because the measured UME current is directly proportional to the rate of H_2 (or O_2) being evolved from the underlying surface, SECM provides a powerful means of mapping out and quantifying differences in H_2 (or O_2) production across a photoelectrode surface.

SECM measurements are performed using nano- or micro-positioners, which typically enable precise control of the X-,Y- and Z- positions of the UME with respect to the sample surface. In addition to SECM maps, which usually provide a qualitative picture of relative charge transport rates at the electrode surface by scanning the UME in the XY-plane, quantitative information, such as the values of kinetic rate constants, can be obtained by fitting SECM approach curve measurements in which the UME current is measured as a function of tip/substrate distance.[49] In PEC systems, the UME and substrate signals are also highly dependent on the ability of photo-generated minority carriers to reach the surface of the photoelectrode, a process that must precede the catalytic charge-transport step. For this reason, SECM in PEC systems is not only sensitive to the spatial variation in catalytic activity at the electrode/electrolyte interface, but also to the optoelectronic properties of the photoelectrode and illumination conditions associated with the experimental set-up.

The type of light source and the means by which light is introduced into the experimental PEC cell are important for SECM measurements of photoelectrode surfaces. Figure 2 depicts four different set-ups for PEC SECM - each of which has advantages and disadvantages. Figure 2a shows a conventional vertically oriented UME being used in conjunction with a light source that illuminates the entire analysis area. While this orientation is fairly straightforward to implement with conventional SECM systems and mimics the uniform illumination of a photoelectrode by sunlight, the arrangement has the drawbacks of partially shadowing the photoelectrode with the UME and more easily supersaturating the electrolyte with the product gas, resulting in gas bubbles that can interfere with SECM measurements. Shadowing by the UME can be especially problematic for approach curves or mapping measurements with very small tip/substrate separation distances, but could be overcome by the use of back illumination of an optically thin photoelectrode,[53,54] as shown in Figure 2b. Alternately, a set-up based on local illumination can be used. For example, in Figure 2c, a focused laser-beam is combined with a diagonally-mounted conical-shaped UME[30] in a set-up that allows for minimization of shadowing effects and background signal arising from the oxidation/reduction of H_2 or O_2 that would normally diffuse from neighboring illuminated areas. However, this approach is limited to monochromic laser light and could more easily lead to high-level carrier-injection conditions. Figure 2d illustrates a combined UME/light source consisting of an optical fiber core that has been metallized to form an annular UME at the end of the fiber.[55–57,12] This apparatus has been successfully used to screen arrays of photocatalytic materials, but such an arrangement inherently possesses reduced spatial resolution due to the ring-geometry of the UME. Modification of an NSOM tip with a similar geometry to that of Figure 2d offers an interesting opportunity to obtain nano-scale resolution for both SECM and SPCM.

The spatial resolution of SECM depends strongly on the radius of the exposed UME tip, a, and the distance between the UME and the electrode surface, d. The normalized tip/substrate separation distance, $L = d/a$, is an important factor because the redox species through which the UME/substrate interaction is mediated can diffuse into or out of the tip/substrate gap. Diffusion of redox active species between the UME and substrate impacts both the spatial resolution and the temporal resolution, so it is generally desirable to minimize the tip/substrate separation distance without actually contacting the surface. UMEs having 1-25 μm diameter tips are routinely employed, and are commercially available, although UME tips as small as 10 nm have been demonstrated.[58,59] SECM thus offers exciting opportunities to study photoelectrode materials and architectures with nano-scale heterogeneities, but the complexity of these measurements often increases substantially at the nano scale.[60–62] Because SECM is typically operated with tip/substrate separation distances that are approximately 1-2 times the tip radius, operating a nano-scale UME at constant Z-position requires that a sample be extremely flat in order to maintain a constant tip/substrate separation distance. If variations in the height of sample features are large compared to the tip/substrate gap distance, it becomes very difficult to distinguish differences in UME current caused by topology rather than electrochemical activity. When the desired UME tip/substrate separation distance is comparable to the roughness of the sample surface, several advanced versions of SECM may be employed, including scanning-force microscopy[63], hybrid SECM/atomic-force microscopy (AFM),[64,65] intermittent-contact SECM,[66,60,61] and electron transfer/ion transfer SECM.[67]

Although this section has focused on the implementation of SECM for the analysis of the spatial variation of product formation on photoelectrode surfaces, SECM can also be used to investigate local changes in pH and[68] corrosion processes,[69–74] analyze surface coverage of adsorbed intermediates (surface interrogation SECM),[75–79] and measure short-lived intermediates.[80,53] When used in conjunction with SPCM, SECM also offers an interesting possibility to semi-quantitatively measure the local faradaic efficiency of photoelectrodes. For instance, the overall photocurrent for an oxygen-evolving photoanode could be due to a combination of two Faradaic processes – anodic photo-corrosion and oxygen evolution. By appropriate choice of UME tip material and applied electrochemical potentials, the SECM tip can be made to be selective to only the oxygen evolved at the substrate; hence, the light-to-oxygen efficiency can be calculated. SECM, in conjunction with SPCM, can also be used for elucidating the dynamics of photo-generated carriers and to map out the spatial distribution of sites of product generation. For instance, due to the heterogeneity of catalytic sites on the photoelectrode surface, the photo-generation of carriers and their collection at the interface need not happen at the same location but could occur at sites that are distant from each other.[30] In such studies, the SECM tip and the SPCM probe can be operated independently to gain additional mechanistic information on the operation of the system of interest.

As SECM is increasingly applied to the study of PEC systems, the use of numerical modeling tools such as finite-element methods to help aid in the interpretation of SECM measurements should be critically pursued, with a foundation provided by similar demonstrations in non-PEC SECM studies.[81–84,52]

2.3 Electrochemical Scanning Tunneling Microscopy

Electrochemical scanning-tunneling microscopy (ECSTM) is an SPM technique used to map the local electron density at surfaces with atomic resolution.[85] As in conventional STM, ECSTM images are generated by measuring spatial variation in electrical signal due to quantum mechanical tunneling of electrons between a substrate and a nano-scale probe tip. Measurements are typically performed in a three-electrode configuration using a bipotentiostat to control the bias of the tip and substrate relative to a suitable reference electrode.[86,87] ECSTM experiments can be undertaken using one of two feedback mechanisms: in constant height mode a fixed tunneling bias voltage is applied between the tip and substrate, while the tunneling current is measured at a fixed tip-sample distance. Alternatively, in constant current mode feedback is used to adjust the voltage applied to the z-axis piezoelectric positioner to move the tip to maintain the specified tunneling current. Constant height mode is typically used for fast scanning of flat surface segments, while constant current mode can be used where the surface topography is less well-defined.[88] Detailed accounts of the experimental set-up and control of ECSTM and STM instruments can be found in literature.[87,89–91]

For small tip-substrate distances (e.g. 1-3 A), the tunneling process reflects the overlap between the electron density of the frontier orbitals of the tip and substrate, while at larger tip-substrate separations the tunneling process can be strongly influenced by the composition and structure of the intervening medium.[85] At even larger tip-substrate distances, electron transfer takes place exclusively through electrochemically-mediated processes, whereby Faradaic charge transfer occurs and the STM measurement merges with SECM methods.[92–94] When STM is performed in vacuum, *tunneling current* vs. *distance* curves can be used to determine the effective work function of the system, while in electrolytes the effective conduction or valence band of the tunneling medium determines the barrier height.[95,96] Such barrier-height measurements have been coupled with potential-dependent imaging studies and theoretical calculations to provide the most detailed description yet of the electronic structure of the double-layer ranging from the influence of simple anionic adsorbates to resonant tunneling through redox active sites including metal centers in proteins.[96–98] The electrochemical double-layer and surface adsorbates are known to influence the band alignment and photovoltage of the photoelectrode, and ECSTM provides an excellent opportunity to directly measure these effects. In particular, *scanning tunneling spectroscopy (STS)* enables the electronic structure of the electrode interface to be examined by varying the tunneling voltage bias in the STM measurement at a fixed tip-substrate separation.[85] With suitable alignment of the tip and substrate Fermi levels, current may be channeled into or out of surface states, the conduction band, or the valence band. The measurements record conductance, which is proportional to the local density of states at different electron energies and enables surface states and/or band edge positions to be determined with nanometer scale spatial resolution. This method has been implemented to understand the electronic structure of semiconductor surfaces in vacuum - although care must be taken to evaluate the impact of tip-induced band bending effects.[99,100] Limits imposed by electrolyte stability and tip reactivity have hampered the application of STS in electrolytic systems. Nevertheless, the power of the method under ambient laboratory conditions was shown in early studies of *n*-TiO_2 and *n*-FeS_2 in air.[101,102] More recently, improvements in tip coating procedures have enabled in-situ collection of tunneling spectra from semiconducting passive films formed by anodization of Fe and Cu.[103,104]

Presently, the biggest challenges of using ECSTM relate to limited knowledge of the structure, composition and stability of the probe tip and underdeveloped insight into tip screening effects that includes the overlap of the respective double layers within the tip-substrate junction. Much of the ECSTM work to date has relied on pattern recognition to interpret the atomic and molecular scale features within images. However, numerous vacuum STM and ECSTM studies show that the tip state plays a significant role in image contrast.[105] Not surprisingly, image simulation plays a central role in interpreting vacuum STM data. In contrast, image simulation in ECSTM remains constrained by the absence of tip definition. Tip preparation and coating procedures have been improved with time, although obtaining a predictable yield of tips capable of atomically resolved imaging remains a challenge and little effort has been made to characterize the structural nature of as-formed tips. Tip materials have a limited potential window that is determined by parasitic Faradic processes ranging from corrosion to electrolyte breakdown. For aqueous electrolytes such phenomena limit the tip-substrate bias potential to values less than ± 1.5 V and thereby restrict full exploration of the energy states associated with wide band gap materials. In contrast, the larger potential widow associated with non-aqueous electrolytes and ionic liquids will enable more extensive use of STS.[106]

A significant constraint on ECSTM is that in order to achieve a single tunnel junction, the substrates of interest must be very flat relative to the curvature of the probe tip. For suitably prepared substrates, *in situ* atomically-resolved imaging of metal and semiconductor electrode surfaces is possible, and with close attention to the operating conditions, potential-dependent surface dynamics such as step motion, surface diffusion, surface alloying, etc., can be followed.[107] A variety of means are available for preparing metal and semiconductor surfaces that range from annealing procedures to electropolishing and etching. Two-dimensional (2-D) layered or van der Waals solids, such as transition-metal dichalcogenides, are materials of long-standing interest in photoelectrochemistry, are now the focus of renewed interest in both electronics and energy research.[108] Fortuitously, such materials are almost ideal for STM studies, as extended atomically flat regions are easily obtained by mechanical cleavage of the substrate. Beyond the challenges of substrate and tip preparation, ECSTM experiments can also be limited by the mechanical stability of the microscope (vibration) and minimization of thermal drift. In conventional STM microscopes the limited scanning speed of constant tunneling current feedback circuitry and the mechanical stability limit the temporal resolution of STM. However, several video rate ECSTM microscopes are now operational and are capable of tracking the trajectory of mobile adsorbates, phase transitions and related defect dynamics in real time.[90,91,107,109]

2.4 Atomic Force Microscopy

One of the most commonly employed SPM techniques is atomic force microscopy (AFM), in which a nanoscale tip is attached to a force-sensing cantilever probe and rastered across a sample surface while the force of the interaction between the tip and the sample is measured.[110,111] AFM is capable of accurately measuring surface morphology at nanometer resolution, or more recently, even with atomic resolution. Additionally, variations of AFM measurements based on conductive tips can enable measurements of local conductivity, capacitance, surface potentials, and more.[112] Beyond vacuum systems, AFM is widely used in the laboratory ambient. Of particular interest are *in situ, in operando* studies of immersed interfaces under electrochemical control (EC-AFM).[113] EC-AFM has been particularly useful for monitoring changes in morphology of semiconductor surfaces due to corrosion,[114,115] including in the photoelectrochemical environment.[114,116] The use of EC-AFM to better understand corrosion and other degradation mechanisms of photoelectrodes could be very useful for the PEC field. *In situ* conductive probe AFM (cp-AFM) has been used to investigate the influence of nano-scale surface defects and morphology on the photoelectrochemical properties of rutile (001) surfaces of n-TiO_2,[117] and more recently used to study local variation in photocurrent and photo-conductivity of individual $CuInSe_2$/Au nanowire heterostructures.[118] Other exciting opportunities to apply *in situ* AFM techniques towards photoelectrochemistry include *in situ* patterning and modification of electrode surfaces[117,119] and elucidation of the electrolyte double layer structure and its associated charge at electrode surfaces.[120–125] Of particular interest are recent AFM studies that have demonstrating the ability to obtain three-dimensional (3D) force maps at a solid-liquid interface that reveal hydration layer structure and dynamics with Angstrom- and sub-minute resolutions, respectively.[122,125] When applied to studying a photoelectrode surface, this application of AFM could be invaluable, not only for better understanding electrochemical charge transfer kinetics, but also the affect that charged species in the electrolyte may have on the space charge layer of photoelectrodes. As discussed in Section 5.2, *in situ* EC-AFM can also be of great use when it is employed simultaneously with other SPM techniques such as SECM.[113] For example, the topological information from AFM can serve as valuable feedback when the property measured by another SPM technique, such as SECM, is highly sensitive to the probe-surface separation distance.

2.5 Optical Spectroscopy Techniques

Unlike conventional electron-based spectroscopies, optical and vibrational spectroscopies such as Raman, infrared (IR), second-harmonic generation (SHG), sum-frequency generation (SFG), photoluminescence (PL), and ultraviolet-visible (UV-Vis) methods, do not require an ultra-high vacuum (UHV) environment, and can be readily coupled with electrochemical measurements using cells with appropriately designed windows that allow optical access to the working electrode.[126] UV-Vis and near infrared (NIR) spectroscopy are particularly useful for spectral assignment of photogenerated species at semiconductor photoelectrodes and for revealing photocarrier transfer/recombination dynamics with high temporal resolution. Such pump-probe methods are discussed in detail in Section 3. Vibrational spectroscopies are well suited for identifying adsorbed molecules, including intermediates, and for providing information regarding the environment around the species of interest.

Among the various vibrational spectroscopies, Raman and surface-enhanced Raman spectroscopy (SERS) are particularly useful for *in situ* studies of photoelectrode surfaces with high lateral spatial resolution, and thus form the focus of this section. Other vibrational spectroscopic techniques such as infrared reflection-absorption spectroscopy (IRAS)[127–129] and SFG[130–132] are also of great interest due to their ability to probe the molecular structure of solvent and adsorbate molecules at electrode surfaces, but can be limited by low sensitivity, energy restrictions that largely exclude the detection of lower frequency modes characteristic to metal/adsorbate complexes, and surface selection rules that exclude detection of adsorbate intramolecular vibrations that are oriented parallel to the interface. Raman spectroscopy is based on the inelastic scattering of light by a molecule or a solid, with the energy shifts of the scattered photons corresponding to quantized transitions in vibrational levels (molecule) or optical phonons (solids). Because the Raman spectrum originates from vibrational transitions, the Raman peaks are numerous and narrow, which makes Raman spectroscopy suitable for molecular “fingerprinting,” compositional mapping, as well as measurement of crystallographic orientation, disorder, and local strain.[133] Unlike its cousin IR spectroscopy, the spectral location of Raman peaks depend on the incident photon energy, and when UV or visible excitation is used, the signals are not affected by water and do not require special 'window' materials such as KBr. For these reasons, Raman spectrometers are found in many teaching, research and industrial institutions, where they are routinely used for identification and structural studies of organic and inorganic compounds.[134] For *in situ* water-splitting applications, Raman has the additional advantage in that the excitation source is a laser, and therefore, Raman spectra can be collected simultaneously with SPCM measurements, thus providing an opportunity to interrogate both the chemical and structural nature of active sites in real time. Furthermore, by using excitation energies either above or below the semiconductor band gap, it may be possible to deduce the nature of the surface adsorbates that are formed by PEC processes.

A principal weakness of Raman spectroscopy is the relatively low scattering cross section for inelastic compared to elastic (Rayleigh) scattering, the latter being ~10^3-10^6 times stronger than the former. For most materials, the small cross section for Raman scattering necessitates the use of long sampling times and/or high laser power to obtain acceptable signal-to-noise. However, the Raman signal can be significantly enhanced by coupling the incident and/or scattered light to localized surface plasmons. Localized surface plasmon resonance (LSPR) is a well-recognized phenomenon in noble metal nanoparticles and nanostructured surfaces due to collective oscillation of conduction electrons under optical excitation, and has been exploited for a variety of applications, including (electro)catalysis.[135–139] When optically excited, the surface plasmons re-emit their energy radiatively (i.e. scattering) at their resonant wavelength or non-radiatively (i.e. absorption) by creating electron-hole pairs. Electromagnetic fields strongly enhanced at nano-protrusions or nano-gaps of a plasmonic material through a localized "antenna" effect cause strongly amplified scattering by adsorbed molecules. The resonant wavelength not only depends on the free electron density and the dielectric constant of the material, but also on the size, geometry, and dielectric constant of the surrounding medium. Because researchers often have control of these parameters, surfaces may be 'tuned' to match the excitation source[8]. In surface-enhanced Raman spectroscopy (SERS), the Raman signal of surface-adsorbed molecules is enhanced by as much as 10^{14}, enabling single molecule detection.[140] The molecular specificity and the rich vibronic information afforded by SERS has enabled numerous recent studies of reaction mechanisms at solid/gas and solid/liquid interfaces.[109] Coupled with the intrinsic merits of Raman spectroscopy, SERS allows adsorbate vibrational spectra to be obtained over wider frequency ranges than either IRAS or SFG, and is also characterized by more relaxed surface-selection rules, thus allowing detection of most vibrational modes irrespective of the molecular orientation.

A limitation of SERS is that the substrate morphology and composition play key roles in producing the SERS effect. Researchers often utilize samples with roughened, nano-structured surfaces, which can be prepared by several means including chemical and electrochemical etching, deposition on pre-patterned substrates, and noble metal coating of polystyrene nanospheres dispersed on glass slides (Fig. 3a and b).[141,142] Because the majority of electrocatalytically relevant metals such as Pt, Rh or Ni do not efficiently sustain surface plasmons, they are coated as ultrathin layers onto plasmonically active Au or Ag nanostructures. Although the catalyst metal overlayer attenuates a fraction of the plasmon-generated electric field, sufficient intensity penetrates to the metal/electrolyte interface to allow identification of adsorbed species and to reveal their degree of charge transfer.[136] An alternate approach was recently used whereby anatase TiO_2 flakes were dispersed onto Al_2O_3 coated plasmonic Ag nanocubes (Fig. 3d). The method was able to identify several reaction intermediates including hydroperoxo (Ti–O–OH), terminal and bridged hydroxo (Ti–OH) and peroxo (Ti–O–O–Ti) intermediates during PEC-based water oxidation.[143] This strategy is similar to the shell-isolated nanoparticle-enhanced Raman spectroscopy (SHINERS), in which Raman scattering is amplified by gold nanoparticles encapsulated with ultrathin silica shells. The latter method can be applied to almost any surface (Fig. 3c). SHINERS has also been used to interrogate metal/electrolyte interfaces.[144] Plasmonic nanostructures have been used in a number of studies to enhance the optical absorption close to the electrochemical interface and thus improve PEC efficiency, particularly at longer wavelengths that typically have low inherent absorption of the semiconductor photoelectrode.[145–147] Characterizing such hybrid photoelectrodes with Raman spectroscopy is an excellent opportunity to elucidate structure-property relationships in these PEC systems.

2.6 Other SPM techniques

Scanning Electrochemical Mass Spectrometry- *In situ* mass spectrometric measurements, such as differential electrochemical mass spectrometry (DEMS), afford chemically specific detection of product, reactant, spectator, or corrosion species at an electrode surface. These techniques have been employed to establish mechanisms and quantify product distributions for electrocatalytic reactions.[148–154] Currently, a disadvantage of most of these techniques is the inability to detect non/semi-volatile reaction products. This drawback arises from the low permeability of the porous Teflon membrane, which separates the vacuum inlet from the solution, to these species. A spatially sensitive variant of the technique is of obvious interest in chemically specific local detection of products, *viz.* H_2 and O_2 at photoelectrodes during water splitting. Scanning-DEMS (SDEMS), employing a scanning vacuum inlet capillary for mass spectrometric detection, has been demonstrated; however, the spatial resolution is on the order of few hundred microns.[155–157] Alternately, the inlet capillary position can be kept constant while the sample is scanned beneath it.[152] In both cases, the resolution of scanning electrochemical mass-spectrometry may be improved through the use of modified multi-barrel nano/micro-capillary tips that have been developed for scanning electrochemical cell microscopy (SECCM).[158,68]

pH-sensing Microscopy- A shared feature of the hydrogen and oxygen evolution reactions is the consumption or production of protons (H^+) or hydroxyls (OH^-) and an associated change in the local pH at the electrode surface. Many corrosion processes are also accompanied by pH changes. Hence, local pH measurements can provide valuable insights into the stability and the activity of photoelectrodes. Fluorescence-based pH-sensing typically involves an optically-excited pH-sensitive chromophore whose change in fluorescence is indicative of the change in local pH. Fluorescence has been previously employed to demonstrate macroscale spatial variations in pH during electrocatalytic reactions at surfaces[159] and for high throughput screening of electrocatalyst libraries.[160] Improved spatial resolution can be realized by the use of a confocal laser-scanning microscope to detect fluorescence.[161,162] Alternately, the application of a pH-sensitive tip in a SECM setup can be used to perform pH-sensing microscopy with micro/nano-scale resolution.[68]

Electron-based *in situ* SPM Techniques- One means of improving the resolution of optical SPM techniques is to replace the optical probe with an electron probe, which can be focused to nanometer or better length scales. Besides providing high spatial resolution, electron-based SPM techniques provide rich and detailed information regarding the structure, composition and electronic states of solid surfaces, and have been used for decades to unravel mechanisms of surface catalytic reactions.[163] One such electron-based SPM technique is electron-beam-induced current (EBIC), which is similar to SPCM except that an electron beam, rather than optical beam, is used to create electron/hole pairs and generate current in a semiconducting material. EBIC is typically performed in vacuum or gas-phase environment, but it is possible to perform EBIC in liquid solution through use of a special test cell in a scanning-electron microscope (SEM) capable of imaging under ambient pressures.[164,165] Efforts are underway to extend vacuum based techniques such as EBIC to probe electrochemical interfaces *in situ*,[166,167] and offer an exciting opportunity to understand PEC processes at the nano-scale. One of the key challenges is to maintain a sufficiently thin liquid electrolyte layer relative to the mean free path of the electrons produced by accelerating voltage in use. For instance if a 30 keV electron beam is employed, the electrolyte layer must be ~30 nm thick.

3. *In situ* Techniques for Evaluation of Photoelectrodes with High Temporal Resolution

Many electronic processes in photoelectrodes, such as photoexcitation, cooling, trapping, recombination, and interfacial transfer of charge carriers, occur on sub-nanosecond time scales, and thus proceed too rapidly to be resolved by electrical measurements.[19] Ultrafast spectroscopic techniques can probe optical, electronic, or vibrational signatures on the requisite femtosecond to nanosecond time scale to directly interrogate these physical phenomena. Figure 4(a) illustrates the basic concept of a pump-probe measurement, whereby a photoexcitation pump pulse is followed after a controlled time delay by a probe pulse. Figure 4(b,c) provides an overview of the different photophysical events in an example TiO_2-Pt system, along with an approximation of the relevant time scales for each event. For other materials systems, time scales for recombination and reactions can also be in the sub-nanosecond range. Bench-scale pump-probe methods generally use Ti:Sapphire lasers as the light source, with pulse durations that are commonly <50 fs. These pulses can be manipulated using non-linear optics to probe either absorption or emission over a spectral region ranging from the ultraviolet to the far-infrared (terahertz frequencies). The diversity of methods enables measurement of carrier lifetimes, transient photoconductivity, and charge transfer kinetics, among other phenomena. This section primarily focuses on transient absorption spectroscopy (TA), the most widely employed ultrafast method to date. An extensive review of ultrafast carrier dynamics for solar fuels formation has been recently published.[13]

TA probes the change in absorption upon photoexcitation as a function of the pump-probe delay time. Probing band-to-band transitions in the visible region reveals the electron and hole populations, while probing a sample in the IR region provides insight into molecular vibrations and/or conductive free carriers. Standard TA configurations focus the optical probe to ≈300 micron spot size, although optical microscope configurations such as those commonly employed in SPCM measurements can reduce the analysis area to length scales close to the optical diffraction limit. For example, TA measurements have been performed using a scanning focused laser beam to perform transient absorption microscopy (TAM) for imaging micron-sized features on graphene oxide.[33] The time resolution is limited by the duration of the laser pulse, often ~50 fs. The maximum time delay depends on the length of the optical delay line, and is typically several nanoseconds. Alternatively, electrical detection using a pulsed pump and a continuous probe allows measurement above nanosecond time scales, with the maximum time determined by the laser repetition rate. Ultrafast measurements require many laser shots to sample the desired time window with sufficient signal-to-noise ratio. Data collection often requires tens of minutes, and samples must be stable for many turnovers under high photon fluxes. Samples should also return to their ground state before the next laser pulse arrives. As with SPCM techniques, the high photon fluxes commonly employed in ultrafast spectroscopies pose a challenge when extrapolating conclusions drawn from ultrafast spectroscopy to systems operating under standard 1-sun conditions. Pulse durations are short and sparse in time (~100 fs pulse repeated every millisecond), but the instantaneous power is very high, often resulting in initial photoexcited carrier densities that are 10-1000 times larger than under steady state 1-sun conditions, and which can place the system in the high-level injection regime.

Most of the early ultrafast spectroscopy studies of electronic materials were performed in air, but recently *in situ* TA has provided additional insight into charge-carrier dynamics. *In situ* measurements present new opportunities to probe the photoelectrode-electrolyte interface under applied bias. Additionally, ultrafast spectrometers using optical delay lines to access the fs – ns time window can be stitched together with data from spectrometers using digital delays with a ns – µs window, and with oscilloscope-based detection and continuous probes with µs – s window to provide gap-free TA spectroscopy over timescales from femtoseconds to seconds. In a recent study of hematite (α-Fe_2O_3), the current-voltage (I-V) characterization under pulsed laser illumination showed the expected improvement in absorbed-photon-to-electron collection efficiency (APCE) under positive applied potentials, but the magnitude of the APCE was significantly lower than under 1-sun conditions because of excessive electron-hole recombination during the initial period of high photoexcited carrier densities.[168] Additionally, *in situ* spectroelectrochemistry was used to assign spectral features to electrons and holes in the visible region and free carriers in the mid-IR, then TA was used to probe the time evolution of these features over fs – µs time windows.[168] A feature at 570 nm was assigned to holes, and decayed at a rate that was independent of applied bias, which indicated that the catalytic activity of the electrodes was determined by holes with lifetimes longer than microseconds. This conclusion agrees with that obtained by *in situ* microsecond TA spectroscopy, which revealed the presence of holes with lifetimes as long as seconds.[169] The lifetime of photogenerated holes increased with applied bias; and a linear relationship between TA amplitude at 200 ms and photocurrent indicated the importance of long-lived holes in the photo-oxidation of water by Fe_2O_3.

Several other ultrafast techniques in addition to TA spectroscopy are of potential interest for investigating PEC materials. Time-resolved terahertz spectroscopy (TRTS) and time-resolved microwave conductivity (TRMC) have been used to measure transient photoconductivity in semiconductors and oxides,[170,171] including such relevant materials as Cu_2O and $BiVO_4$.[172,173] In both of these methods, the conductivity is probed using far-infrared radiation. TRTS provides information on ultrafast (ps – ns) time scales, while TRMC probes the dynamics on ns - µs time scales. Both types of probes are strongly absorbed by water and conductive electrolytes, so *in situ* experiments are challenging. However, special cell designs utilizing a back-illumination configuration or very thin electrolyte layers in a recirculating scheme to avoid build-up of photoproducts may be effective. Other ultrafast techniques of interest include time-resolved XPS and time-resolved XRD to study the surface and bulk structural changes that result from photoexcitation of the material or an adsorbed sensitizer.[174,175] These methods require a synchrotron source, and *in situ* measurements are likely to be extremely challenging due to the nature of signal detection. Most of the techniques outlined in this paragraph have not been applied extensively for investigations of PEC materials and processes to date, but many opportunities exist to develop new insights through the use of such methods.

4. Modeling and Simulation of Photoelectrode Operation at Small Length and Ultrafast Time Scales

Computational modeling, particularly when informed and validated by the experimental techniques described in the previous sections, can be employed to offer additional insights into the key processes that underlie operation of PEC photoelectrodes, and ultimately use that knowledge to predict new, high performance PEC materials. Unlike the experimental techniques discussed up to this point, there exist many well-established and readily available computational modeling tools for simulating PEC possesses at sub-nm length scales *and* fs/ps time scales. While high spatial and temporal resolution are easily obtained with computational tools, the key challenge becomes that of "realistic" modeling of photoelectrodes under conditions that most closely approximate actual device operation.[176] In this regard, computational modeling can operate hand-in-hand with *in situ* experimental characterization techniques, with the latter providing the needed insights into electrode structure, chemistry, and dynamics during operation. Given recent advancements in both high-performance computing and computational algorithms, opportunities for using modeling and simulation as predictive tools for PEC studies are expanding.[177–179,18,180,17] Accordingly, it is becoming increasingly evident that modeling and characterization efforts require tighter integration as PEC research activities move forward.

Figure 5 illustrates schematically three stages of PEC operation that must be considered for accurate computational modeling of the entire reaction: the initial reaction setup (e.g., surface/interface formation), illumination, and final product formation. Note that the latter two stages generally overlap with the steps in Figure 4, encompassing photoabsorption, carrier generation and re-equilibration, charge transfer, and chemical reactivity. The first stage involves understanding how a material responds to exposure to the environment.

The key challenge in accurately modeling the entire PEC process is that the individual contributing processes in Figure 5 operate at intrinsically different length and time scales that cannot be treated using a single theoretical method. For instance, carrier generation and mobility usually occur in the fs regime, whereas the catalytic charge-transfer reaction is typically much slower and the recombination/release/photocorrosion steps can be much slower still. Moreover, the results of each stage depend on those of the previous stage: the reaction chemistry and kinetic pathway depends on the instantaneous interfacial structure of the photoexcited electrode surface, which in turn depends on the chemistry of the electrode surface upon electrolyte immersion. This interdependency makes it difficult to predict with any certainty what the outcome will be, since uncertainties in each stage are propagated throughout the reaction. The solution to these difficulties is twofold. First, computational methods that provide different tradeoffs between accuracy and computational expense and that operate at different scales must be combined. Second, the simulations must rely on accurate experimental probes of processes and local structures to provide input and validation to the models and minimize error propagation, particularly during the later stages of the reaction.

Broadly speaking, computational methods can be separated into continuum and atomistic approaches. In general, continuum approaches provide superior flexibility for studying device operation, and are capable of accessing much broader ranges of length and time scales. They are also well suited for examining operation under non-equilibrium conditions and examining the overall kinetics of interdependent reaction stages, which facilitates more direct comparison with experimentally accessible quantities. However, continuum approaches provide little or no information about the atomic-level details of interface structure or chemistry, relying instead on parameterization by atomistic or experimental approaches. On the other hand, atomistic approaches are better suited for understanding mechanisms and chemical interactions, since they treat atoms and molecules explicitly. The disadvantage is that they are limited in the scales of systems that can be accessed, and generally neglect broader features such as microstructure, surface/interface inhomogeneity, interfacial band bending, and variations in electrolyte composition.

In this section, we describe the use of atomistic computational methods to accurately model physiochemical processes in operating PEC systems and better understand the mechanistic details that underlie PEC operation at small length and ultrafast time scales. We do not discuss continuum-based approaches that could be adapted for kinetic modeling of PEC operation; towards this end, there are a number of recent publications and reviews describing the specific application of continuum models to the properties and performance of photoelectrodes.[181–187] Nevertheless, it should be emphasized that one of the most pressing current research needs in the PEC community is the development of simulation frameworks that combine the power and accuracy of atomistic approaches with the flexibility of continuum approaches. This would allow for simulation of the kinetics of PEC operation at the system level under "realistic" conditions of varying pH, illumination, bias, and electrolyte composition/concentration. As such unified simulation frameworks become available, the atomistic techniques we describe may be combined with continuum approaches to further bridge the gap between theory and experiment.

4.1. DFT and ground-state techniques

Density functional theory (DFT) in its various flavors has emerged as the primary workhorse of first-principles computational materials science.[188] Providing arguably the most favorable tradeoff between computational cost and accuracy, DFT has been applied widely to study the chemistry and electronic structure of photoelectrode materials and their surfaces.[189,180] It has also been used extensively to study surface catalytic reactions, particularly in the context of descriptor-based optimization and high-throughput screening of candidate water oxidation and proton reduction electrocatalysts.[190–194] Moreover, there are several methods available that can use DFT-derived energetics to directly compute reaction barriers and extract free energy surfaces. These include the nudged elastic band (NEB)[195] and metadynamics approaches,[196] which have found extensive usage in investigating water redox and dissociation reactions on photocatalyst and photoelectrode materials.[197–204]

An additional advantage of ground-state techniques such as DFT and *ab initio* molecular dynamics (AIMD) is that these techniques are also available for simulating spectroscopic quantities that can be compared directly with experimental probes, particularly at PEC interfaces. These include computation of IR/Raman spectra,[205–207] as well as XAS/XES[208–211] spectra. Methods that require explicit treatment of excited states, such as UV-Vis/IR optical spectroscopy, are covered in the next section. These experimental techniques offer a viable pathway for model validation.

Historically, much of the DFT-based work has focused on studying bulk electrodes and their idealized surfaces in vacuum. Recently, there has been growing interest in extending the application of DFT to study *interfaces* between electrodes and electrolytes, which require large simulation cells that can treat both components on equal footing. This trend can be considered analogous to the adoption of *in situ* techniques in experimental characterization. Typically, consideration of the liquid electrolyte also requires explicit treatment of atomistic dynamics in an *ab initio* molecular dynamics scheme (AIMD; alternatively, first-principles MD or DFT-MD), which relies on DFT-computed forces to propagate atomic trajectories. Examining interfaces using DFT is further complicated by a general lack of understanding of how surfaces and surface reconstructions form in solution as compared to their vacuum counterparts. Nevertheless, several groups have adopted AIMD approaches to study the structure and chemistry of semiconductor-water interfaces for PEC applications.[212,197,213,214,200,215–224] The presence of semiconductor surfaces often significantly alters the dynamical and chemical properties of water; conversely, the presence of the electrolyte can significantly alter the physiochemical properties of the semiconductor. Accordingly, recent simulations have reported a wide variety of complex chemical processes active at semiconductor surfaces when liquid water is included explicitly, such as water dissociative adsorption,[197,213,200,215–217,221,223,220] surface hydroxylation and radical formation,[197,213,200,215–218,222,220] unusual changes in the hydrogen-bond network,[212,197,213,214,200,215–219] and fast surface proton hopping.[197,213–216] It is also possible to assess surface acidity/basicity based on AIMD simulations of water-semiconductor interfaces when water dissociation is active.[225,216,213] Collectively, these reports point to the importance of the specific interaction between the electrode and the electrolyte in determining the physiochemical properties of the interface and the associated reaction mechanisms, and highlight the future need for consideration of both species in accurate models of PEC operation.

An alternative to explicit inclusion of the full electrolyte in AIMD simulations is to describe some portion of the electrolyte using an implicit solvation scheme that combines traditional DFT with polarizable continuum models. This approach has long been used in the quantum chemistry community to study ionic and molecular solvation,[226] and similar ideas are now beginning to be adapted for solid-liquid interfaces.[227–231]. Such polarizable continuum-based schemes can also mitigate another critical challenge for realistic simulations of electrode-electrolyte interfaces and catalytic redox electrochemistry—namely, the application of a well-defined voltage bias or photo-bias. Typically, there are two complications associated with an external bias within DFT: first, charge neutrality considerations that prevent accurate determination of a potential reference for a charged system that can be directly compared with experiments; and second, fundamental incompatibilities with the periodic boundary conditions generally employed for simulations of extended crystalline systems. Specific approaches for dealing with these shortcomings have been outlined within the context of the effective screening medium (ESM),[230,231] joint DFT (JDFT) [232–234] and self-consistent continuum solvation (SCCS)[229,235] methodologies. Alternative schemes for defining universal potential references for PEC-relevant reactions in DFT/AIMD have also been proposed.[236–238]

Implementations of the abovementioned techniques are rather new, and in most cases their application has been confined to metallic electrodes. Nevertheless, they present a promising approach for considering [photo]voltage-dependent electronic, dynamical, and structural effects observed at semiconductor-liquid PEC interfaces during operation. One example is the complex relationship between the structure and dynamics of the electric double layer and the space-charge effect it induces on the charged photoelectrode. They also open up the possibility of directly examining the mechanisms and kinetics of charge-transfer reactions at PEC interfaces under bias. In this latter case, one must be careful to consider the distinction between the more commonly employed constant-charge scheme and the more experimentally relevant constant-potential scheme.[239] The recently proposed potentiostat method of Bonnet and Otani[231] is an example of a constant-potential scheme that could be implemented directly within AIMD to permit dynamics at a fixed bias that better represents experimental conditions in a PEC cell.

Despite their predictive power, conventional DFT and AIMD have some significant theoretical limitations that are relevant for investigations of PEC materials. One of these is an inability to correctly describe charge localization, particularly in strongly correlated electronic systems. This shortcoming can prove particularly problematic for simulating charge transport within many transition-metal oxides, where conductivity may be driven by a polaronic hopping mechanism rather than direct band transport (e.g., alpha-Fe2O3).[189,240–242] In such systems, charge transport is often the rate-limiting process, making accurate theoretical description paramount. To a large extent, this limitation can be overcome by adoption of more advanced exchange-correlation functionals that include some amount of exact Hartree-Fock exchange (so-called hybrid functionals)[243,222] or Hubbard corrections (DFT+U).[244] The appropriate amount of exact exchange or +U to include is generally system dependent, and can be determined empirically or else directly from ab-initio calculations.[245–248] In the case of hybrid functionals, the additional computational expense can also significantly limit AIMD simulation times, particularly when applied to solid-liquid interfaces. Second, DFT is inherently a ground-state method, and thus cannot in general provide an accurate description of excited-state properties.

For instance, it is well-known that DFT underestimates band gap and cannot quantitatively valence and conduction band edge positions.[249,236] It also prevents treatment of electronic excited-state dynamics and true photoillumination conditions.[176] Accordingly, it is better suited to examining interfaces in the dark, although the next section provides a brief overview of excited-state and beyond-DFT methods that can be incorporated to address this limitation.

Occasionally, it may become necessary to determine quantities such as adsorbate binding energies and dissociation barriers with even higher accuracy than DFT can generally provide (for instance, to be used as inputs in coarse-grained or model-Hamiltonian approaches). In these cases, more advanced methods may be invoked at the cost of additional computational expense. These include higher-order perturbative quantum chemical methods,[250,251] as well as Quantum Monte Carlo (QMC),[252] which solves the electronic wavefunction stochastically. These methods are currently limited in the system sizes they can access and are difficult to implement in a dynamics framework, and have therefore not been widely applied to PEC materials. However, a more realistic use may be for benchmarking DFT calculations on model systems and informing the proper choice of DFT exchange-correlation functionals, or else for systematic refinement of energetics.

4.2. Excited-state and beyond-DFT methods

Proper simulation of the optical excitations associated with photoelectrode illumination or with optical probe techniques requires augmenting ground-state DFT with higher-order methods that consider electronic excited states. An overview of these methods is included in this section, and a more detailed discussion can be found in a recent review by Ping *et al.*[176] In general, excited-state methods carry significantly higher computational expense than ordinary ground-state DFT, and are therefore limited to much smaller systems and time scales. One of the most popular excited-state methods is the extension of the ground-state DFT formalism known as time-dependent DFT (TDDFT),[253–255] which relies on full solution of the time-dependent Schrödinger equation within a set of prescribed approximations. TDDFT allows one to simulate oscillator strengths and vertical excitations for all relevant electronic transitions. It can therefore be used to describe the optical absorption spectrum of a model photoelectrode, or to understand how bulk absorption states change at surfaces or interfaces. In addition, TDDFT-based approaches can provide excited-state electron dynamics in the fs regime, which is a useful tool for directly simulating ultrafast pump-probe experiments. Such techniques may enable investigations of charge carrier dynamics that are directly relevant to PEC devices, including interfacial charge transfer between co-catalysts and photoabsorbers, or through semiconductor-insulator-metal junctions. To date, probably the most mature application of TDDFT to photoelectrode materials has been in the context of carrier injection and transport in dye-sensitized TiO_2.[256–258]

For certain semiconductors, TDDFT may be inadequate for accurately predicting photoexcitation spectra.[176,255] In these instances, more accurate determination of electronic excitations can be achieved using methods based on many-body perturbation theory and the

Green's function formalism.[259] The GW approximation is the current state-of-the-art for the calculations of quantities obtained from photoemission spectroscopy measurements (PES, XPS), such as semiconductor band gaps and band edge alignments.[260] Similarly, the Bethe-Salpeter (BSE) equation, which employs two-particle Green's functions, provides a reliable approach for describing optical absorption processes that involve electron-hole interactions.[261] Historically, these techniques have been considered too expensive for application to PEC interfaces; however, recent algorithmic developments[262–264] allows one to apply the GW method to larger system sizes, permitting direct treatment of both the solid electrode and liquid electrolyte.[265–269] This opens up opportunities to investigate how local electronic states are altered by the presence of the liquid electrolyte within a formalism that is often more robust than TDDFT, and provides a possible template for comparison with high-resolution experimental probes. As alternatives to the GW/BSE approach, high-level quantum chemistry methods such as Møller–Plesset perturbation theory (MPn),[270] coupled cluster theory (CC),[271] configuration interaction (CI),[272] complete active space self-consistent field (CASSCF),[273] and complete active space with second-order perturbation theory (CASPT2)[274] can be employed to calculate excited-state properties. To date, these approaches have been applied primarily to molecules and nanostructures.[275,276] Developments to extend these approaches to study solids are underway; however, further advances are required before they can be used to study PEC interfaces.[277,278]

Although TDDFT, GW, and BSE techniques can be used to determine the electronic structure of a photoelectrode material upon optical excitation, they do not provide the excited-state dynamics of atoms and ions. To this end, a promising emerging direction involves coupling excited-state electronic dynamics (in particular, TDDFT) with AIMD to investigate the effect of photoexcitation on the nonadiabatic dynamical evolution of the surface atoms and adsorbates.[279–281,258] One such implementation was recently applied by the Prezhdo group to study nonadiabatic processes in photoinduced water splitting on GaN,[282] and has found similar successes in studies of photocatalytic processes on metal oxides.[258] Naturally, the simulation times that can be achieved are limited by the time scale of the electron dynamics (fs regime), but ultrafast responses can be studied. At present, it is unclear under which conditions such nonadiabatic atomic responses can be relevant to the reaction mechanisms on PEC photoelectrodes, but it represents an exciting future research pathway.[258]

4.3. Coarse-grained, model-Hamiltonian, and force-field approaches

Among the most significant limitations of DFT-based techniques is an inability to access the larger length (beyond a few nm) and time scales (beyond hundreds of ps) required to investigate later reaction stages or to fully describe variations in the electrode microstructure or electrolyte composition. As discussed above, a possible solution is to combine atomistic approaches with continuum approaches. However, in the absence of a unified framework, atomistic approaches that take advantage of coarse graining, simplified model Hamiltonians, and parameterized classical potentials can also push closer to accessing more realistic system sizes and much longer simulation times.

Classical molecular dynamics approaches based on interatomic potentials that are fit to experimental or *ab initio*-derived properties represent one option for scaling to > μm system sizes and > ns simulation times. These techniques make it possible to account for the full composition and evolution of the liquid electrolyte (even at low ion concentrations or weakly acidic/alkaline conditions, which typically require very large simulations), as well as many features in the electrode microstructure. However, a key difficulty lies in the proper parameterization of the interatomic potentials, which must be valid not only for describing bulk properties of the electrode and electrolyte, but also the interface between the two. By contrast, AIMD is based on first-principles descriptions that are agnostic to the chemical environment. A second obstacle that is particularly relevant to PEC hydrogen or oxygen evolution is the inability of most classical dynamics frameworks to properly treat chemical reactions that involve bond breaking and forming. Currently, the most attractive solution to these difficulties is to use methods based on reactive classical potentials/force fields that are specifically designed to permit bond breaking/forming and are "trained" using data from smaller AIMD runs. In recent years, the ReaxFF technique[283] has emerged as the best known reactive force-field method, and has been successfully applied to the study of a few semiconductor-liquid interfaces.[284–286] However, additional work on training ReaxFF potentials using AIMD needs to be done in order to improve the transferability and predictive power of such techniques for other photoelectrode materials, particularly given the sensitivity of the potential parameters to the particular surface and electrolyte composition.

Alternatively, one can abandon real-time dynamics in favor of stochastic approaches that offer insight into PEC reaction kinetics and transport processes based on model Hamiltonians. One of the most powerful model-Hamiltonian techniques is kinetic Monte Carlo (kMC), which can take advantage of *ab initio*-derived reaction and diffusion barriers (e.g., from DFT or QMC) to predict overall reaction kinetics. Techniques based on kMC are attractive because they are extraordinarily flexible and capable of accessing wide ranges of timescales depending on the specific level of spatiotemporal discretization. However, they generally rely on decomposing PEC reactions into well-defined reaction steps, each with a well-defined barrier. Given the inherent complexity and inhomogeneity of semiconductor-electrolyte interfaces, this can be extremely difficult in practice. Nevertheless, when used appropriately, kMC is well suited to offer semi-quantitative descriptions of reaction kinetics and charge transport processes that can be directly compared with experimental probes. For instance, kMC techniques have been used to study charge transport in hematite[287] and through grain boundaries in polycrystalline TiO_2.[288] The latter example illustrates how kMC can be applied to amorphous systems based on an averaged homogeneous description, which presents extraordinary challenges for conventional DFT-based models that rely on actual atomic configurations. Model-Hamiltonian techniques have also been adopted to refine PEC reaction barriers in the presence of the liquid electrolyte. An excellent example is the approach introduced by Santos *et al.*,[289] which uses an Anderson-

Newns model in conjunction with ordinary DFT to predict proton abstraction barriers. This same method was recently successfully applied to the catalytic hydrogen evolution on the PEC electrode material MoS_2.[290]

Another issue that can plague DFT studies of photoelectrode surfaces is the complexity in surface structure and atomic arrangement, particularly for alloys, defect- or adsorbate-rich surfaces, and amorphous or polycrystalline electrodes. Similar challenges exist for examining atomic structures at the solid interface between the semiconductor and the catalyst. There is currently no definitive solution to these difficulties, emphasizing the need for high-fidelity experimental characterization to inform atomistic models. Nevertheless, approaches have typically relied on decomposing the material into local building blocks that can be computed explicitly, which are then combined to generate and predict new low-energy structures. This can be done by qualitative observations of local chemical similarities in simplified models,[291] or else by using rigorously defined mathematical methodologies. In the latter category, one of the most popular approaches is the cluster expansion method,[292] which has been applied successfully to efficiently determine bulk and surface alloy compositions of crystalline photoelectrode materials.[293–297] The cluster expansion method relies on mapping the compositional variation onto an Ising-like lattice-gas model Hamiltonian, each "site" of which may be independently occupied (or unoccupied) by a given substitutional species. Accordingly, its accuracy depends on the reliability of the lattice-gas mapping, which is limited to well-defined bulk or surface structures. For instance, it can be adapted to study lattice point defects, but it is not suitable for amorphous materials. The lattice-gas assumption must also be rigorously verified for PEC surfaces in an electrolyte solution, which can be highly dynamic and facilitate large atomic rearrangements.

5. Special Topics

5.1 Coordinating high resolution *in situ* measurements with traditional, macro-scale measurements

Although the *in situ* experimental techniques discussed in this article can provide valuable information about photoelectrode properties at small length and fast time scales, the experimental conditions for these measurements are often very different from those involved with real device operating conditions. For example, differences in the local and global reaction rates, in addition to differences in the intensity, uniformity, and spectral characteristics of the light source, are common. Hence, results obtained from nano- or micro-scale measurements must be extrapolated with suitable caveats to predict or explain macroscopic photoelectrode performance under AM 1.5 operating conditions. When possible, nano/micro and macro measurements should be performed under similar conditions. Unfortunately, trade-offs are often present between signal-to-noise ratio, resolution, and mimicking realistic PEC device operating conditions. For both nano/micro and macro-scale measurements, data can be collected over a range of operating conditions, such as light intensity or applied potential, to ascertain the sensitivity of the measured differences in behavior to operating conditions and thus gain insight into the validity of direct quantitative comparison between measurements at different length scales.

Scanning-probe measurements are necessarily local measurements, the output of which will naturally vary across the macroscopic surface. The variation in a measured property across a macroscopic sample surface can be quantified by performing the high resolution measurement at multiple microscopic regions, as is commonly done in electron microscopy. Having performed local SPM measurements at multiple locations, variation in the nano or micro-scale signal can be compared with macro-scale measurements. Whenever possible, observations and conclusions drawn from micro- and nano-scale measurements should be cross-checked by the use of more traditional, macro-scale PEC measurements (e.g., using an AM 1.5 light source) and/or computational modeling tools. Detailed descriptions of the standard protocols for commonly employed macro-scale PEC measurements, such as current-voltage characteristics and quantum yield measurements can be found in the literature.[298,299]

5.2 Combined *in situ* Techniques

All of the SPM techniques in Table I can provide valuable information about photoelectrode materials when performed individually, but a much more complete view of photoelectrode operation can be obtained when multiple SPM techniques are combined in the same measurement platform and performed simultaneously.[300] Such combined or multifunctional *in situ* measurement platforms represent a powerful means of obtaining complementary information that can more easily elucidate complex structure-property relationships. Importantly, performing multiple measurements simultaneously ensures that identical experimental conditions are employed for each technique and on the same nano- or microscopic area of the photoelectrode. In contrast, it can be difficult to achieve identical analytical and electrode surface conditions when two or more independent *in situ* measurements are conducted sequentially, especially if different electrochemical test cells are employed for each technique.

Many examples of combined *in situ* measurements have been demonstrated for electrochemical or photoelectrochemical systems. The combination of SECM with AFM has been used to correlate nano- or micron-scale variation in (photo)catalytic activity to topological features such as grain boundaries, catalyst particles, and more.[300,113,301] Combined AFM/STM enables simultaneous measurements of the force and conductance curves of two impinging double layers in the electrochemical environment, while the natural pairing of Raman mapping and SPCM offers the ability to investigate variations in local photocurrent as a function of the chemical or physical nature of the photoelectrode surface. Other examples of combined *in situ* measurements that have been reported include SPCM/SECM,[55,12,57,30,302] SPCM/shear force topography,[44] SECM/AFM,[300] and Raman/SPCM,[303] SECM/optical microscopy(OM),[304,305] ECSTM/SECM,[93,94,306] NSOM/fluorescence spectroscopy,[307,308] and ECSTM/TERS.[309,310] The capabilities of these various multifunctional set-ups are vast, and their usefulness will vary substantially from material to material, making some set-ups better suited than others for investigating certain PEC materials and/or chemistries.

6. Conclusions and Future Outlook

The continued development of experimental and computational techniques to study photoelectrochemical systems with high spatial and temporal resolution can provide a more complete understanding of fundamental PEC processes and thus aid in the development of commercially viable PEC technology. This review has described several types of experimental and computational tools that are well-suited for achieving these objectives. Particular emphasis has been placed on experimental techniques that can investigate photoelectrode properties *in situ*, providing valuable information about properties and performance in the photoelectrochemical environment. Scanning probe measurement techniques are especially useful for interrogating photoelectrodes at small length scales, while time resolved pump-probe spectroscopy techniques are well-suited for studying PEC processes at very fast time scales. Atomistic modeling tools provide the ability to unlock mechanisms of PEC processes at the smallest length and fastest time scales, which in many cases are not currently accessible with experimental techniques. When informed by and used in coordination with experimental techniques, computational techniques may offer PEC researchers unique abilities to discover and design photoelectrode materials through an understanding of photoelectrode operation.

Nearly all of the techniques described in this review possess major challenges or limitations in their successful application to PEC systems. Many techniques have inherent limitations on length and time scales that can be described, or are only compatible with certain materials and/or photoelectrode morphologies. Another key challenge in the development of *in situ* experimental techniques and computational tools for studying PEC systems at small length and time scales is their application at operating conditions that are relevant to real-world PEC operation under AM 1.5 illumination. Improvement in hardware, software algorithms, and experimental set-ups germane to current techniques will continue to be important for overcoming these limitations, as will the careful coordination of multiple experimental and computational techniques to bridge length and time scales. Together, these approaches will enable a suite of tools that should significantly accelerate the discovery, design, and optimization of materials for solar-driven water splitting with photoelectrochemical cells.

Acknowledgements

We acknowledge the helpful assistance of the DOE-EERE PEC H2 Working Group. A summary version of this review paper can be found on the working group website (http://energy.gov/eere/fuelcells/photoelectrochemical-working-group) as well as tables that are being updated as the PEC field progresses. JMV, JJ, and NSL would like to acknowledge the

Joint Center for Artificial Photosynthesis, a DOE Energy Innovation Hub, supported through the Office of Science of the U.S. Department of Energy under Award No. DE-SC0004993 and the National Science Foundation Grant CHE-1214152. JMV acknowledges support through a NRC Ford Foundation Postdoctoral Fellowship.. BW and TO acknowledge support from the Fuel Cell Technologies Program within the DOE Office of Energy Efficiency and Renewable Energy. A portion of this work was performed under the auspices of the U.S. Department of Energy by Lawrence Livermore National Laboratory under Contract DE-AC52–07NA27344. Sandia is a multi-program laboratory operated by Sandia Corporation, a Lockheed Martin Company, for the U.S. DOE National Nuclear Security Administration under Contract DE-AC04-94AL85000. AAT was supported by Science of Precision Multifunctional Nanostructures for Electrical Energy Storage (NEES), an Energy Frontier Research Center funded by the U.S. Department of Energy, Office of Science, and Office of Basic Energy Sciences under award DESC0001160.

Tables

Table I. Experimental techniques suitable for *in situ* evaluation of photoelectrodes with high spatial and/or temporal resolution. This list is not exclusive, but intended to highlight key classes of techniques that have already been successfully applied to the study of photoelectrode materials or offer clear opportunities for future research efforts.

Technique	**Probe type**	**Key properties measured**	**Typical resolution**	**Limitations and challenges**
Scanning photocurrent microscopy (SPCM) (Conventional)	Optical	Locally generated photocurrent; used to determine local quantum efficiency, minority carrier diffusion lengths, electric field distributions, and more	1-25 μm	Spatial resolution set by Abbe diffraction limit; typically limited to monochromatic light; avoiding high injection conditions and bubble formation
Near Field Scanning Optical Microscopy (NSOM)-based SPCM	Optical/ Physical	Similar capabilities to SPCM, but with higher spatial resolution.	10’s nm-1 μm	Spatial resolution set by size of NSOM tip aperture; tip heating; interference; difficult on rough surfaces
Optical spectroscopies (Raman, UV-Vis, IR, SFG)	Optical	Chemical, physical, and optical properties of photoelectrode surface	1-25 μm	Spatial resolution set by Abbe diffraction limit; long acquisition times; bubble formation
Ultrafast spectroscopies e.g. transient absorption spectroscopy (TA)	Optical	Lifetimes of electronic and vibrational states, interfacial charge transfer rates, and transient photoconductivity (THz)	sub ps – ns, 100 μm	Long acquisition times; avoiding high injection conditions; different detection systems for <ns, ns – μs, and μs – s
Scanning electrochemical microscopy (SECM)	Physical / electrochemical (non-contact)	Local catalytic activity and kinetic rate constants; sensitive to local opto-electronic properties in PEC systems; advanced forms of SECM for pH-sensing, corrosion analysis, and more	10’s nm – 100 um	Resolution set by tip dimensions and tip-substrate distance; difficult with rough surfaces; bubble formation; challenges with light integration
Electrochemical Scanning Tunneling Microscopy (E-STM)	Physical/ Electronic	Atomically resolved physical and electronic structure; video rate imaging possible	Å –nm (atomic resolution possible)	Difficult on rough surfaces; limited scan area size; poorly defined tip geometries, limited electrochemical window for STM tips
Atomic force microscopy (AFM)	Physical / Electronic	Surface morphology, conductivity, capacitance, surface potentials, double layer forces, hydration layer structure	Å-5 nm (atomic resolution possible)	Difficult on rough surfaces; limited scan area size; limited electrochemical window for conductive tips

Table II. Atomistic theoretical tools suitable for investigation of photoelectrode properties and processes with high spatial and/or temporal resolution and under simulated operating conditions.

Technique(s)	Method type	Key properties determined	Accessible time/ length scales	Limitations and challenges
Density functional theory (DFT) and *ab initio* molecular dynamics (AIMD)	*Ab initio*	Electronic/optical/chemical/mechanical properties, including surface and interface; can provide spectroscopic information (XPS, XAS/XES, Raman/IR); can estimate reaction and diffusion barriers with moderate accuracy; additional improvements possible with corrected exchange-correlation functionals (e.g., hybrid, van der Waals, DFT+*U*).	~100 ps and a few nm (a few thousand atoms)	Limited to relatively small length/time scales; no description of electronic/optical excitations; potential accuracy issues, especially for strongly correlated systems and for prediction of electronic levels; results depend on choice of exchange-correlation functional
Time-dependent density functional theory (TDDFT) and nonadiabatic dynamics	*Ab initio*	Dynamics of photoexcited electrons; can provide information directly comparable to pump/probe ultrafast measurements.	~100 fs and a few nm (a few thousand atoms)	Limitations coming from approximations are not always systematic or well understood; limited to very short time scales
GW/Bethe-Salpeter Equation (BSE)	*Ab initio*	Accurate computation of electron excitation (optical) spectra, band gaps, and absolute band edges; suitable for quantitative comparison with experiments (e.g., photoemission).	Hundreds of atoms	Computationally expensive; no dynamical/temporal information
Quantum Monte Carlo (QMC)	*Ab initio*	Very accurate estimates of adsorption energies, reaction barriers, and band gaps; (can be used to augment and benchmark DFT)	Hundreds of atoms	Computationally expensive; extremely challenging to study dynamics
Classical molecular dynamics and reactive force-field methods	Parameterized	Dynamics can be studied at much larger length and time scales than those accessible to DFT; useful for simulating transport and surface diffusion, collective behaviors, and electrolyte dynamics	≈ 1 ns, millions of atoms	Parameterization and accuracy validation are difficult, particularly for interfaces; barriers and transition states are often inaccurate
Cluster Expansion	*Ab initio* (based on model Hamiltonian)	Thermodynamic stability of bulk and surface alloys, as well as adsorbate configurations; generally based on DFT framework; useful for studying composition of multi-element electrodes	Scalable to 10^3-10^6 atoms, depending on cluster size	Assumes model in which atoms are fixed at defined lattice positions; May require many interaction terms; No dynamical/temporal information
Kinetic Monte Carlo (kMC)	Parameterized (based on model Hamiltonian)	Stochastic method to treat mass transport and reaction kinetics across broad length and time scales; can be used to examine surface diffusion- or reaction-limited processes based on DFT-derived barriers	Arbitrarily scalable	Requires prior knowledge of relevant rate-limiting mechanisms and mapping onto lattice model; Assumes fixed, well-defined barriers for each discrete reaction or transport step

Figures

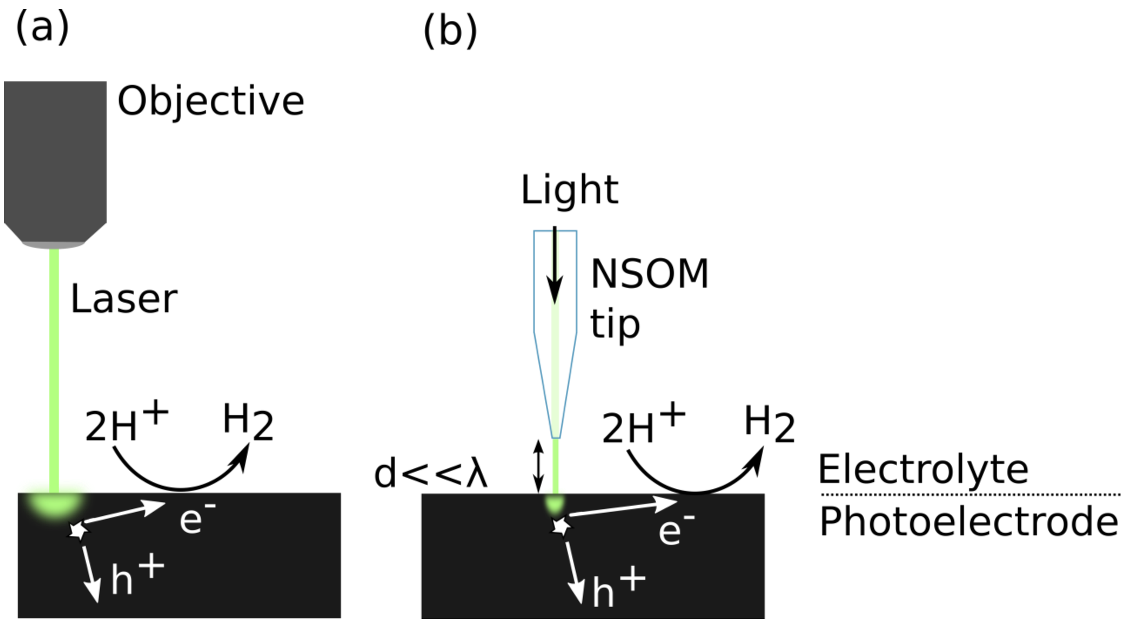
(a)
(b)
Objective
Laser
Light
NSOM
tip
2H+
H2
2H+
H2
d<<λ
Electrolyte
Photoelectrode
e-
h+
e-
h+

Figure 1. Schematics of (a) conventional and (b) NSOM-based SPCM set-ups for *in situ* scanning photocurrent analysis of photoelectrodes for water splitting. Schematics not to scale. Schematics illustrate H_2 evolving from a photocathode surface, but identical illustrations could be drawn for photoanodes evolving O_2. The light green regions in the figure represent the photon absorption / charge carrier generation volume in the semiconducting photoelectrode.

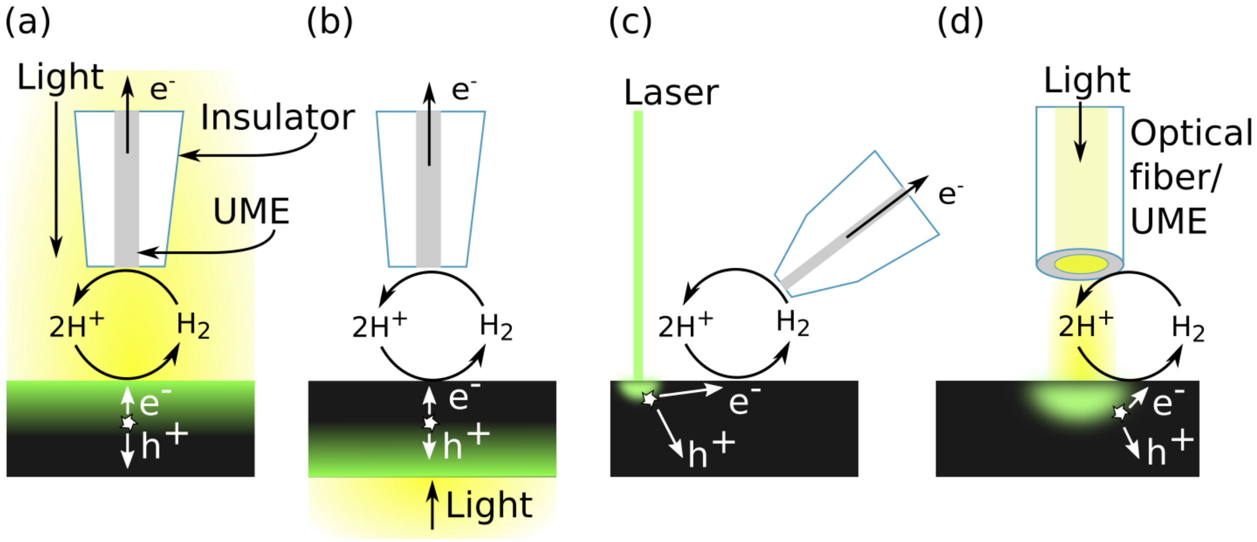
(a)
Light
e⁻
Insulator
UME
2H⁺
H₂
e⁻
h⁺
(b)
e⁻
2H⁺
H₂
e⁻
h⁺
Light
(c)
Laser
e⁻
2H⁺
H₂
e⁻
h⁺
(d)
Light
Optical fiber/ UME
2H⁺
H₂
e⁻
h⁺

Figure 2. Schematic side-views of several SECM set-up arrangements that can be used for investigating photoelectrode surfaces. Schematics not to scale. Schematics illustrate H_2 evolving from a photocathode surface, but identical illustrations could be drawn for photoanodes evolving O_2. The light green regions in the figure represent the photon absorption / charge carrier generation volume in the semiconducting photoelectrode.

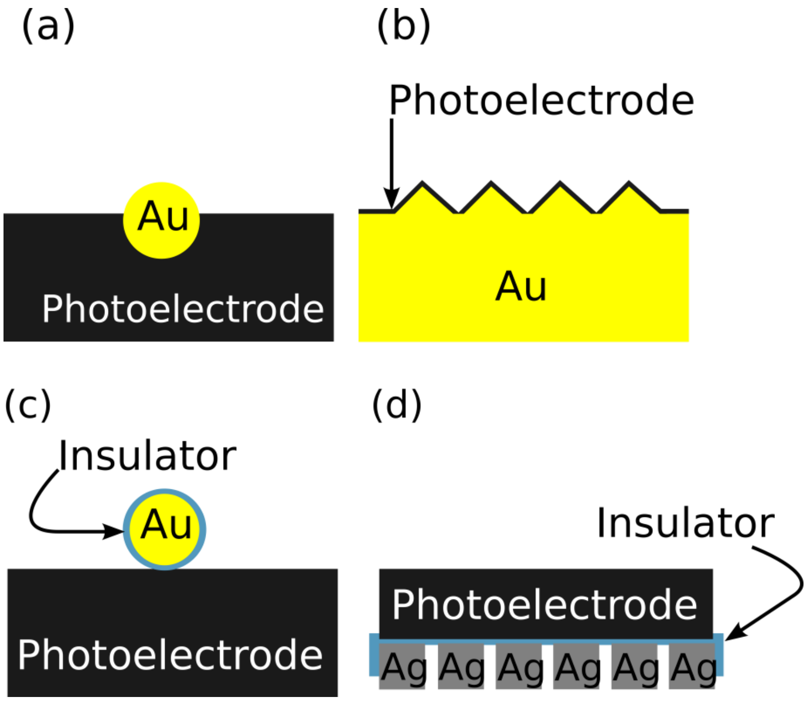
(a)
Au
Photoelectrode
(b)
Photoelectrode
Au
(c)
Insulator
Au
Photoelectrode
(d)
Insulator
Photoelectrode
Ag Ag Ag Ag Ag Ag

Figure 3. Strategies for generating localized surface plasmon resonance on photoelectrode surfaces that could be used for SERS characterization: a) Au nanoparticles embedded in a photoelectrode (after ref. 119); b) Photoelectrode material deposited over Au nanopillars in an "overlayer SERS" configuration (after ref. 120); c) Ultra-thin SiO_2 or Al_2O_3 coated Au nanoparticles deposited over a photoelectrode (after ref. 129); d) PEC material deposited over Ag nanocubes coated with ultra-thin Al_2O_3 insulator (after ref. 128).

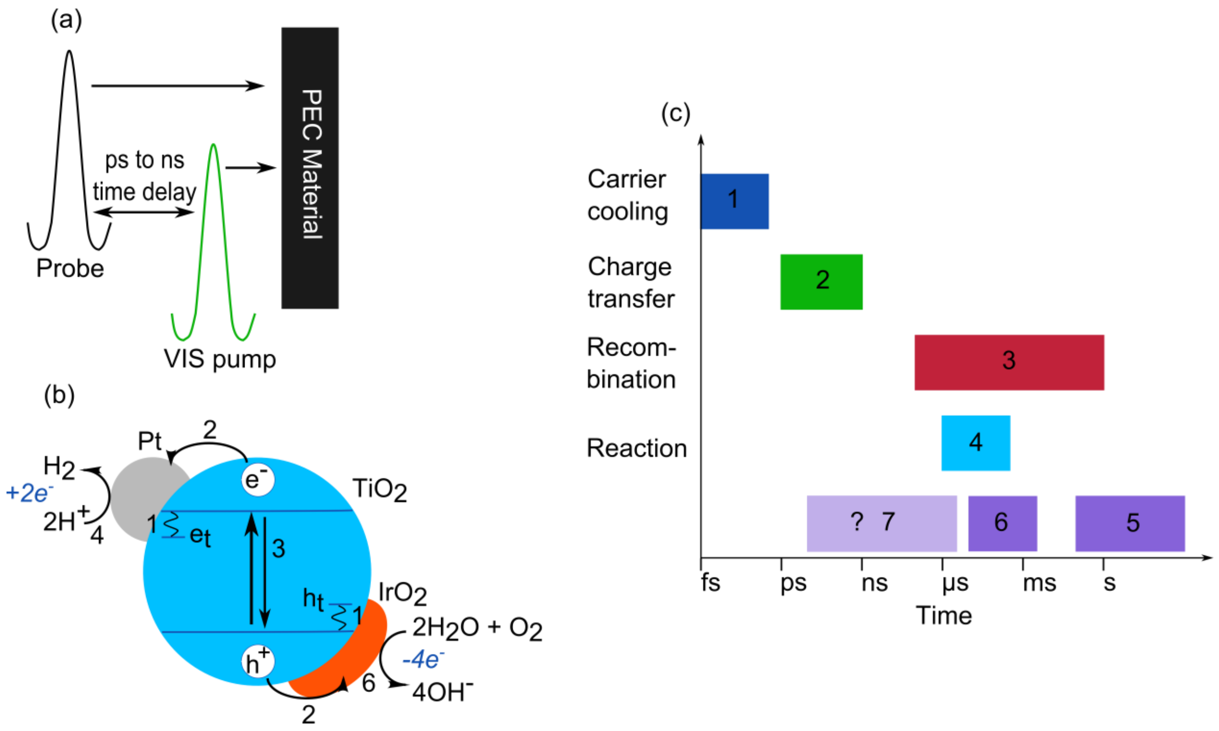
(a)
ps to ns
time delay
Probe
VIS pump
PEC Material
(b)
Pt
2
H2
+2e-
2H+
4
1
et
e-
TiO2
3
ht
1
IrO2
2H2O + O2
-4e-
4OH-
h+
6
2
(c)
Carrier cooling
1
Charge transfer
2
Recom-bination
3
Reaction
4
? 7
6
5
fs
ps
ns
μs
ms
s
Time

Figure 4. (a) Schematic of a generic ultrafast pump-probe spectroscopy experiment. (b) Photophysical processes and (c) their approximate time scales for different steps in PEC water splitting for an example system comprising TiO_2 nanoparticles decorated with Pt and IrO_2 catalytic nanoparticles. Steps include (*1*) carrier cooling and trapping, (*2*) interphase electron transfer from TiO_2 to Pt, (*3*) geminate recombination, (*4*) hydrogen evolution reaction on Pt catalyst, (*5*) O_2 evolution on TiO_2, (*6*) O_2 evolution on Pt, and (*7*) O_2 evolution for next-generation OER catalysts.

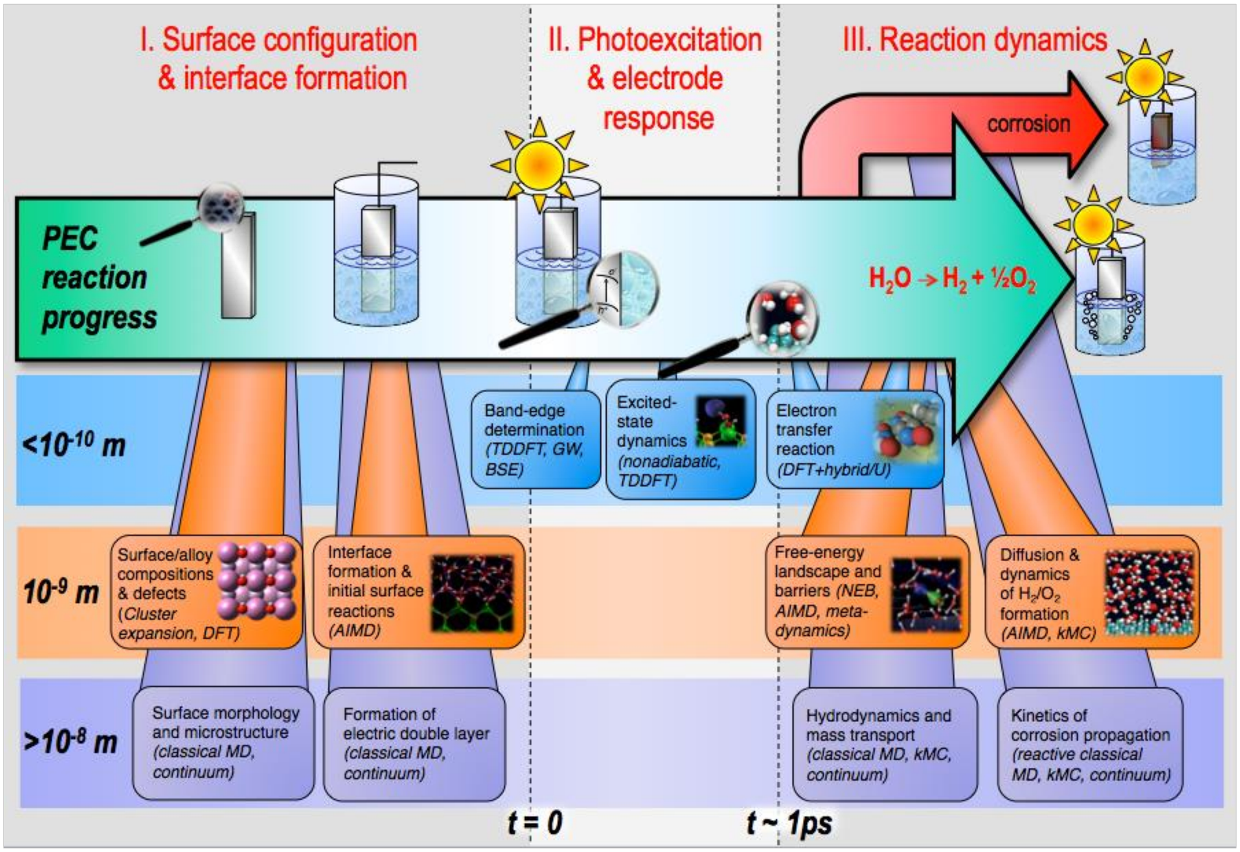
I. Surface configuration & interface formation
II. Photoexcitation & electrode response
III. Reaction dynamics
corrosion
PEC reaction progress
H₂O → H₂ + ½O₂
<10⁻¹⁰ m
10⁻⁹ m
>10⁻⁸ m
Band-edge determination (TDDFT, GW, BSE)
Excited-state dynamics (nonadiabatic, TDDFT)
Electron transfer reaction (DFT+hybrid/U)
Surface/alloy compositions & defects (Cluster expansion, DFT)
Interface formation & initial surface reactions (AIMD)
Free-energy landscape and barriers (NEB, AIMD, meta-dynamics)
Diffusion & dynamics of H₂/O₂ formation (AIMD, kMC)
Surface morphology and microstructure (classical MD, continuum)
Formation of electric double layer (classical MD, continuum)
Hydrodynamics and mass transport (classical MD, kMC, continuum)
Kinetics of corrosion propagation (reactive classical MD, kMC, continuum)
t = 0
t ~ 1ps

Figure 5. Schematic of various processes and stages contributing to the complete PEC water splitting reaction (green arrow), along with possible computational methods for treating the associated physical or chemical phenomena at different length and time scales. The vertical position on the graph corresponds to the relative length scale of the process, whereas the position of the wedge where it intersects with the green arrow indicates its relative time scale.

References

1. M. Gratzel, *Nature*, 2001, **414**, 338–344.

2. J. Turner, G. Sverdrup, M. K. Mann, P. C. Maness, B. Kroposki, M. Ghirardi, R. J. Evans, and D. Blake, *Int. J. Energy Res.*, 2008, **32**, 379–407.

3. M. G. Walter, E. L. Warren, J. R. McKone, S. W. Boettcher, Q. Mi, E. A. Santori, and N. S. Lewis, *Chem. Rev.*, 2010, **110**, 6446–6473.

4. N. S. Lewis, *ECS Interface*, 2013, **22**, 43–50.

5. *US DOE Multi-Year Res. Dev. Demonstr. Plan*, 2012.

6. J. R. McKone, N. S. Lewis, and H. B. Gray, *Chem. Mater.*, 2014, **26**, 407–414.

7. A. Fujishima and K. Honda, *Nature*, 1972, **238**, 37–38.

8. A. Kudo and Y. Miseki, *Chem. Soc. Rev.*, 2009, **38**, 253–278.

9. E. L. Miller, N. Gaillard, J. Kaneshiro, A. DeAngelis, and R. Garland, *Int. J. energy Res.*, 2010, **34**, 1215–1222.

10. X. Chen, S. Shen, L. Guo, and S. S. Mao, *Chem. Rev.*, 2010, **110**, 6503–6570.

11. P. C. K. Vesborg and T. F. Jaramillo, *Rsc Adv.*, 2012, **2**, 7933–7947.

12. J. Lee, H. Ye, S. Pan, and A. J. Bard, *Anal. Chem.*, 2008, **80**, 7445–50.

13. H. Ye, J. Lee, J. S. S. Jang, and A. J. J. Bard, *J. Phys. Chem. C*, 2010, **114**, 13322–13328.

14. G. Liu and A. J. Bard, *J. Phys. Chem. C*, 2010, **114**, 17509–17513.

15. J. H. He and B. A. Parkinson, *Acs Comb. Sci.*, 2011, **13**, 399–404.

16. J. M. Gregoire, C. X. Xiang, X. N. Liu, M. Marcin, and J. Jin, *Rev. Sci. Instrum.*, 2013, **84**.

17. J. Greeley, T. F. Jaramillo, J. Bonde, I. B. Chorkendorff, and J. K. Norskov, *Nat. Mater.*, 2006, **5**, 909–913.

18. I. E. Castelli, T. Olsen, S. Datta, D. D. Landis, S. Dahl, K. S. Thygesen, and K. W. Jacobsen, *Energy Environ. Sci.*, 2012, **5**, 5814–5819.

19. J. B. Baxter, C. Richter, and C. A. Schmuttenmaer, *Annu. Rev. Phys. Chem.*, 2014, **65**, null.

20. N. S. Lewis, *Acc. Chem. Res.*, 1990, **23**, 176–183.

21. A. J. Nozik and R. Memming, *J. Phys. Chem.*, 1996, **100**, 13061–13078.

22. A. Minguzzi, D. Battistel, J. Rodríguez-López, A. Vertova, S. Rondinini, A. J. Bard, and S. Daniele, *J. Phys. Chem. C*, 2015, **119**, 2941–2947.

23. C. Bhattacharya, H. C. Lee, and A. J. Bard, *J. Phys. Chem. C*, 2013, **117**, 9633–9640.

24. K. M. Nam, H. S. Park, H. C. Lee, B. H. Meekins, K. C. Leonard, and A. J. Bard, 2013, 2–5.

25. X. Zhang, H. Li, S. Wang, F. R. F. Fan, and A. J. Bard, *J. Phys. Chem. C*, 2014, **118**, 16842–16850.

26. K. C. Leonard, K. M. Nam, H. C. Lee, S. H. Kang, H. S. Park, and A. J. Bard, *J. Phys. Chem. C*, 2013, **117**, 15901–15910.

27. S. P. Berglund, H. C. Lee, P. D. Núñez, A. J. Bard, and C. B. Mullins, *Phys. Chem. Chem. Phys.*, 2013, **15**, 4554–65.

28. B. Moralejo, M. a. González, J. Jiménez, V. Parra, O. Martínez, J. Gutiérrez, and O. Charro, *J. Electron. Mater.*, 2010, **39**, 663–670.

29. W. Warta, *Sol. Energy Mater. Sol. Cells*, 2002, **72**, 389–401.

30. D. V Esposito, I. Levin, T. P. Moffat, and A. A. Talin, *Nat. Mater.*, 2013, **12**, 562–8.

31. R. Graham and D. Yu, *Mod. Phys. Lett. B*, 2013, **27**, 1330018.

32. E. Abbe, *Arch. für mikroskopische Anat.*, 1873, **9**, 413–418.

33. R. Kopelman and W. Tan, *Science (80-.).*, 1993, **262**, 1382–1384.

34. Q. Wu, G. D. Feke, R. D. Grober, and L. P. Ghislain, *Appl. Phys. Lett.*, 1999, **75**, 4064–4066.

35. Z. Wang, W. Guo, L. Li, B. Luk’yanchuk, A. Khan, Z. Liu, Z. Chen, and M. Hong, *Nat. Commun.*, 2011, **2**, 218.

36. L. Kastrup, H. Blom, C. Eggeling, and S. Hell, *Phys. Rev. Lett.*, 2005, **94**, 178104.

37. V. Westphal and S. Hell, *Phys. Rev. Lett.*, 2005, **94**, 143903.

38. K. Y. Han, S. K. Kim, C. Eggeling, and S. W. Hell, *Nano Lett.*, 2010, **10**, 3199–203.

39. E. Betzig and J. K. Trautman, *Science*, 1992, **257**, 189–95.

40. C. M. Harris, *Anal. Chem.*, 2003, **75**, 223A–228A.

41. C. R. McNeill, H. Frohne, J. L. Holdsworth, J. E. Furst, B. V. King, and P. C. Dastoor, *Nano Lett.*, 2004, **4**, 219–223.

42. M. S. Leite, M. Abashin, H. J. Lezec, A. G. Gianfrancesco, A. A. Talin, and N. B. Zhitenev, *IEEE J. Photovoltaics*, 2014, **4**, 311–316.

43. M. S. Leite, M. Abashin, H. J. Lezec, A. Gianfrancesco, A. A. Talin, and N. B. Zhitenev, *ACS Nano*, 2014, **8**, 11883–11890.

44. L. F. Garfias-Mesias and W. H. Smyrl, *J. Electrochem. Soc.*, 1999, **146**, 2495–2501.

45. S. Kawata, Y. Inouye, and P. Verma, *Nat. Photonics*, 2009, **3**, 388–394.

46. M. Burghard and A. Mews, *ACS Nano*, 2012, **6**, 5752–5756.

47. M. D. Kelzenberg, D. B. Turner-Evans, B. M. Kayes, M. a Filler, M. C. Putnam, N. S. Lewis, and H. a Atwater, *Nano Lett.*, 2008, **8**, 710–4.

48. A. J. Bard and M. V Mirkin, *Scanning Electrochemical Microscopy, Second Edition*, Taylor & Francis, 2012.

49. M. V Mirkin, W. Nogala, J. Velmurugan, and Y. Wang, *Phys. Chem. Chem. Phys.*, 2011, **13**, 21196–212.

50. A. J. Bard and M. V Mirkin, *Scanning Electrochemical Microscopy*, Taylor & Francis, 2001.

51. S. Amemiya, A. J. J. Bard, F.-R. F. R. F. Fan, M. V. V Mirkin, and P. R. R. Unwin, in *Annu. Rev. Anal. Chem.*, 2008, vol. 1, pp. 95–131.

52. P. Bertoncello, *Energy Environ. Sci.*, 2010, **3**, 1620.

53. H. S. Park, K. C. Leonard, and A. J. Bard, 2013.

54. D. Bae, T. Pedersen, B. Seger, M. Malizia, A. Kuznetsov, O. Hansen, I. Chorkendorff, and P. C. K. Vesborg, *Energy Environ. Sci.*, 2015.

55. N. Casillas, *J. Electrochem. Soc.*, 1995, **142**, L16.

56. P. James, *J. Electrochem. Soc.*, 1996, **143**, 3853.

57. W. Liu, H. Ye, and A. J. Bard, *J. Phys. Chem. C,* 2010, **114**, 1201–1207.

58. J. Velmurugan, P. Sun, and M. V. Mirkin, *J. Phys. Chem. C*, 2009, **113**, 459–464.

59. P. Sun and M. V. V Mirkin, *Anal. Chem.*, 2006, **78**, 6526–6534.

60. D. O. Wipf, A. J. Bard, and D. E. Tallman, *Anal. Chem.*, 1993, **65**, 1373–1377.

61. M. a Edwards, A. L. Whitworth, and P. R. Unwin, *Anal. Chem.*, 2011, **83**, 1977–84.

62. K. McKelvey, M. A. Edwards, P. R. Unwin, and K. M. Kelvey, 2010, **82**, 6334–6337.

63. S. E. Pust, M. Salomo, E. Oesterschulze, and G. Wittstock, *Nanotechnology*, 2010, **21**, 105709.

64. H. Shin, P. J. Hesketh, B. Mizaikoff, and C. Kranz, *Anal. Chem.*, 2007, **79**, 4769–77.

65. J. Wiedemair, B. Balu, J. Moon, D. W. Hess, B. Mizaikoff, and C. Kranz, *Anal. Chem.*, 2008, **80**, 5260–5.

66. K. McKelvey, M. A. Edwards, and P. R. Unwin, *Anal. Chem.*, 2010, **82**, 6334–7.

67. Y. Wang, K. Kececi, J. Velmurugan, and M. V. Mirkin, *Chem. Sci.*, 2013, **4**, 3606.

68. B. P. Nadappuram, K. McKelvey, R. Al Botros, A. W. Colburn, and P. R. Unwin, *Anal. Chem.*, 2013, **85**, 8070–4.

69. A. Davoodi, J. Pan, C. Leygraf, and S. Norgren, *Electrochem. Solid-State Lett.*, 2005, **8**, B21.

70. K. Eckhard, M. Etienne, A. Schulte, and W. Schuhmann, *Electrochem. commun.*, 2007, **9**, 1793–1797.

71. T. E. Lister and P. J. Pinhero, *Electrochim. Acta*, 2003, **48**, 2371–2378.

72. R. M. Souto, Y. González-García, and S. González, *Corros. Sci.*, 2005, **47**, 3312–3323.

73. N. Casillas, S. J. Charlebois, W. H. Smyrl, and H. S. White, *J. Electrochem. Soc.*, 1993, **140**, L142–L145.

74. P. I. James, L. F. Garfias-Mesias, P. J. Moyer, and W. H. Smyrl, *J. Electrochem. Soc.*, 1998, **145**, L64–L66.

75. J. Rodríguez-López, M. a Alpuche-Avilés, and A. J. Bard, *J. Am. Chem. Soc.*, 2008, **130**, 16985–95.

76. J. Rodríguez-López and A. J. Bard, *J. Am. Chem. Soc.*, 2010, **132**, 5121–9.

77. Q. Wang, J. Rodríguez-López, and A. J. Bard, *J. Am. Chem. Soc.*, 2009, **131**, 17046–7.

78. B. H. Simpson and J. Rodríguez-López, *Electrochim. Acta*, 2015.

79. B. H. Simpson and J. Rodríguez-López, *Anal. Methods*, 2015.

80. M. Zhou, Y. Yu, K. Hu, and M. V. Mirkin, *J. Am. Chem. Soc.*, 2015, 150515154407005.

81. P. R. Unwin and A. J. Bard, *J. Phys. Chem.*, 1991, **95**, 7814–24.

82. A. J. Bard, M. V Mirkin, P. R. Unwin, and D. Wipf, *J. Phys. Chem.*, 1992, **96**, 1861–1868.

83. F. Zhou, P. R. Unwin, and A. J. Bard, *J. Phys. Chem.*, 1992, **4924**, 4917–4924.

84. C. J. Slevin, J. V Macpherson, and P. R. Unwin, *J. Phys. Chem. B*, 1997, **101**, 10851–10859.

85. C. J. Chen, *Introduction to Scanning Tunneling Microscopy Second Edition*, Oxford University Press, New York, NY, 2008.

86. D. . Kolb, *Surf. Sci.*, 2002, **500**, 722–740.

87. I. V. Pobelov, C. Li, and T. Wandlowski, in *Encyclopedia of Nanotechnology*, 2012, pp. 688–702.

88. P. K. Hansma and J. Tersoff, *J. Appl. Phys.*, 1987, **61**, R1–R23.

89. M. Wilms, M. Kruft, G. Bermes, and K. Wandelt, *Rev. Sci. Instrum.*, 1999, **70**, 3641.

90. M. J. Rost, L. Crama, P. Schakel, E. van Tol, G. B. E. M. van Velzen-Williams, C. F. Overgauw, H. ter Horst, H. Dekker, B. Okhuijsen, M. Seynen, A. Vijftigschild, P. Han, A. J. Katan, K. Schoots, R. Schumm, W. van Loo, T. H. Oosterkamp, and J. W. M. Frenken, *Rev. Sci. Instrum.*, 2005, **76**, 053710.

91. Y. I. Yanson, F. Schenkel, and M. J. Rost, *Rev. Sci. Instrum.*, 2013, **84**, 023702.

92. M. V Mirkin, F. R. Fan, and A. J. Bard, *Science (80-.).*, 1992, **257**, 364–366.

93. O. Sklyar, T. H. Treutler, N. Vlachopoulos, and G. Wittstock, *Surf. Sci.*, 2005, **597**, 181–195.

94. H. Wolfschmidt, D. Weingarth, and U. Stimming, *ChemPhysChem*, 2010, **11**, 1533–1541.

95. O. Pecina, W. Schmickler, K. Y. Chan, and D. J. Henderson, *J. Electroanal. Chem.*, 1995, **396**, 303–307.

96. F. C. Simeone, D. M. Kolb, S. Venkatachalam, and T. Jacob, *Surf. Sci.*, 2008, **602**, 1401–1407.

97. N. J. Tao, *Phys. Rev. Lett.*, 1996, **76**, 4066–4069.

98. J. Zhang, A. M. Kuznetsov, I. G. Medvedev, Q. Chi, T. Albrecht, P. S. Jensen, and J. Ulstrup, *Chem. Rev.*, 2008, **108**, 2737–2791.

99. M. McEllistrem, G. Haase, D. Chen, and R. J. Hamers, *Phys. Rev. Lett.*, 1993, **70**, 2471–2474.

100. H. Yu, L. J. Webb, J. R. Heath, and N. S. Lewis, *Appl. Phys. Lett.*, 2006, **88**, 252111.

101. F. F. Fan and A. J. Bard, *J. Phys. Chem.*, 1990, **94**, 3761–3766.

102. F. Fan and A. J. Bard, *J. Phys. Chem.*, 1991, **95**, 1969–1976.

103. I. Diez-Perez, A. G. Güell, F. Sanz, and P. Gorostiza, *Anal. Chem.*, 2006, **78**, 7325–7329.

104. F. Caballero-Briones, J. M. Arte, I. Diez-Perez, P. Gorostiza, and F. Sanz, *J. Phys. Chem. C*, 2009, **113**, 1028–1036.

105. H. Mo and E. I. Altman, *ACS Nano*, 2013, **7**, 10233–10244.

106. T. Albrecht, K. Moth-poulsen, J. B. Christensen, J. Hjelm, T. Bjørnholm, and J. Ulstrup, *J. Am. Chem. Soc.*, 2006, 6574–6575.

107. M. Giesen, *Prog. Surf. Sci.*, 2001, **68**, 1–153.

108. J. B. Park, B. Jaeckel, and B. A. Parkinson, *Langmuir*, 2006, **22**, 5334–5340.

109. B. Sharma, R. R. Frontiera, A. I. Henry, E. Ringe, and R. P. Van Duyne, *Mater. Today*, 2012, **15**, 16–25.

110. F. J. Giessibl, *Rev. Mod. Phys.*, 2003, **75**, 949.

111. F. J. Giessibl, *Mater. Today*, 2005, **8**, 32–41.

112. A. Avila and B. Bhushan, *Crit. Rev. Solid State Mater. Sci.*, 2010, **35**, 38–51.

113. J. V. Macpherson and P. R. Unwin, *Anal. Chem.*, 2000, **72**, 276–285.

114. O. Nast, S. Rauscher, H. Jungblut, and H.-J. Lewerenz, *J. Electroanal. Chem.*, 1998, **442**, 169–174.

115. H. J. Lewerenz, M. Aggour, C. Murrell, M. Kanis, H. Jungblut, J. Jakubowicz, P. a. Cox, S. a. Campbell, P. Hoffmann, and D. Schmeisser, *J. Electrochem. Soc.*, 2003, **150**, E185.

116. E. Wierzbiński and M. Szklarczyk, *Thin Solid Films*, 2003, **424**, 191–200.

117. T. Miki and H. Yanagi, *Langmuir*, 1998, **14**, 3405–3410.

118. N. J. Economou, S. Mubeen, S. K. Buratto, and E. W. McFarland, *Nano Lett.*, 2014, **14**, 3328–3334.

119. K. Salaita, Y. Wang, and C. a Mirkin, *Nat. Nanotechnol.*, 2007, **2**, 145–155.

120. A. C. Hillier, S. Kim, and A. J. Bard, *J. Phys. Chem.*, 1996, **100**, 18808–18817.

121. J. Wang and A. J. Bard, *J. Phys. Chem. B*, 2001, **105**, 5217–5222.

122. T. Fukuma, Y. Ueda, S. Yoshioka, and H. Asakawa, *Phys Rev. Lett.*, 2010, **104**, 2–5.

123. G. B. Kaggwa, P. C. Nalam, J. I. Kilpatrick, N. D. Spencer, and S. P. Jarvis, *Langmuir*, 2012, **28**, 6589–6594.

124. J. I. Kilpatrick, S. H. Loh, and S. P. Jarvis, *J. Am. Chem. Soc.*, 2013, **135**, 2628–2634.

125. E. T. Herruzo, H. Asakawa, T. Fukuma, and R. Garcia, *Nanoscale*, 2013, **5**, 2678–85.

126. A. J. Bard and L. R. Faulkner, *Electrochemical Methods: Fundamentals and Applications*, Wiley, 2nd edn., 2000.

127. M. Osawa, in *Near-Field Optics and Surface Plasmon Polaritons*, ed. S. Kawata, Springer, Berlin, 2001, vol. 187, pp. 163–187.

128. M. Ito, *Surf. Sci. Rep.*, 2008, **63**, 329–389.

129. M. Osawa, M. Tsushima, H. Mogami, G. Samjeské, and A. Yamakata, *J. Phys. Chem. C*, 2008, **112**, 4248–4256.

130. G. L. Richmond, *Chem. Rev.*, 2002, **102**, 2693–2724.

131. F. Vidal and A. Tadjeddine, *Reports Prog. Phys.*, 2005, **68**, 1095–1127.

132. T. Ishiyama, T. Imamura, and A. Morita, *Chem. Rev.*, 2014, 140328154856008.

133. J. R. Ferraro, K. KNakamoto, and C. W. Brown, *Introductory Raman Spectroscopy*, Elsevier, 2003.

134. D. A. Skoog, F. J. Holler, and T. A. Niemann, *Principles of Instrumental Analysis*, Saunders College Publishing, 1998.

135. A. J. Haes, C. L. Haynes, A. D. McFarland, G. C. Schatz, R. R. Van Duyne, and S. L. Zou, *Mrs Bull.*, 2005, **30**, 368–375.

136. H. Yang, Y. Yang, and S. Zou, *J. Phys. Chem. C*, 2007, **111**, 19058–19065.

137. Z. Q. Tian, B. Ren, Y. X. Chen, S. Z. Zou, and B. W. Mao, *J. Chem. Soc. Faraday Trans.*, 1996, **92**, 3829–3838.

138. S. Linic, P. Christopher, and D. B. Ingram, *Nat. Mater.*, 2011, **10**, 911–921.

139. M. J. Kale, T. Avanesian, and P. Christopher, *ACS Catal.*, 2014, **4**, 116–128.

140. S. Nie and S. R. Emory, *Science (80-.).*, 1997, **275**, 1102–1106.

141. A. Campion and P. Kambhampati, *Chem. Soc. Rev.*, 1998, **27**, 241–250.

142. T. R. Jensen, M. D. Malinsky, C. L. Haynes, and R. P. Van Duyne, *J. Phys. Chem. B*, 2000, **104**, 10549–10556.

143. X. Y. Ling, R. X. Yan, S. Lo, D. T. Hoang, C. Liu, M. A. Fardy, S. B. Khan, A. M. Asiri, S. M. Bawaked, and P. D. Yang, *Nano Res.*, 2014, **7**, 132–143.

144. J. F. Li, Y. F. Huang, Y. Ding, Z. L. Yang, S. B. Li, X. S. Zhou, F. R. Fan, W. Zhang, Z. Y. Zhou, D. Y. Wu, B. Ren, Z. L. Wang, and Z. Q. Tian, *Nature*, 2010, **464**, 392–395.

145. Z. W. Liu, W. B. Hou, P. Pavaskar, M. Aykol, and S. B. Cronin, *Nano Lett.*, 2011, **11**, 1111–1116.

146. I. Thomann, B. A. Pinaud, Z. Chen, B. M. Clemens, T. F. Jaramillo, and M. L. Brongersma, *Nano Lett.*, 2011, **11**, 3440–3446.

147. H. Gao, C. Liu, H. E. Jeong, and P. Yang, *ACS Nano*, 2012, **6**, 234–40.

148. H. Baltruschat, *J. Am. Soc. Mass Spectrom.*, 2004, **15**, 1693–706.

149. A. H. Wonders, T. H. M. Housmans, V. Rosca, and M. T. M. Koper, *J. Appl. Electrochem.*, 2006, **36**, 1215–1221.

150. J. Gun, S. Bharathi, V. Gutkin, D. Rizkov, A. Voloshenko, R. Shelkov, S. Sladkevich, N. Kyi, M. Rona, Y. Wolanov, M. Koch, S. Mizrahi, P. V. Pridkhochenko, A. Modestov, and O. Lev, *Isr. J. Chem.*, 2010, **50**, 360–373.

151. P. Liu, M. Lu, Q. Zheng, Y. Zhang, H. D. Dewald, and H. Chen, *Analyst*, 2013, **138**, 5519–39.

152. J.-P. Grote, A. R. Zeradjanin, S. Cherevko, and K. J. J. Mayrhofer, *Rev. Sci. Instrum.*, 2014, **85**, 104101.

153. A. a. Topalov, S. Cherevko, A. R. Zeradjanin, J. C. Meier, I. Katsounaros, and K. J. J. Mayrhofer, *Chem. Sci.*, 2014, **5**, 631.

154. A. Bharti, P. C. Ma, and R. Salgia, *Mass Spectrom. Rev.*, 2015, **26**, 451–466.

155. K. Jambunathan and a. C. Hillier, *J. Electrochem. Soc.*, 2003, **150**, E312.

156. K. Jambunathan, S. Jayaraman, and A. C. Hillier, *Langmuir*, 2004, **20**, 1856–1863.

157. E. D. Rus, H. Wang, A. E. Legard, N. L. Ritzert, R. B. Van Dover, and H. D. Abruña, *Rev. Sci. Instrum.*, 2013, **84**, 024101.

158. N. Ebejer, A. G. Güell, S. C. S. Lai, K. McKelvey, M. E. Snowden, and P. R. Unwin, *Annu. Rev. Anal. Chem. (Palo Alto. Calif).*, 2013, **6**, 329–51.

159. W. J. Bowyer, J. Xie, and R. C. Engstrom, *Anal. Chem.*, 1996, **68**, 2005–9.

160. E. Reddington, *Science (80-.).*, 1998, **280**, 1735–1737.

161. N. C. Rudd, S. Cannan, E. Bitziou, I. Ciani, A. L. Whitworth, and P. R. Unwin, *Anal. Chem.*, 2005, **77**, 6205–17.

162. a. J. Leenheer and H. a. Atwater, *J. Electrochem. Soc.*, 2012, **159**, H752–H757.

163. G. A. Somorjai, *Chemistry in Two Dimensions: Surfaces*, Cornell University Press, 1981.

164. J. L. Keddie, P. Meredith, R. a. L. Jones, and a. M. Donald, *Macromolecules*, 1995, **28**, 2673–2682.

165. S. Thiberge, A. Nechushtan, D. Sprinzak, O. Gileadi, V. Behar, O. Zik, Y. Chowers, S. Michaeli, J. Schlessinger, and E. Moses, *Proc. Natl. Acad. Sci. USA*, 2004, **101**, 3346–3351.

166. F. El Gabaly, M. Grass, A. H. McDaniel, R. L. Farrow, M. A. Linne, Z. Hussain, H. Bluhm, Z. Liu, and K. F. McCarty, *Phys. Chem. Chem. Phys.*, 2010, **12**, 12138–12145.

167. A. Kolmakov, D. A. Dikin, L. J. Cote, J. X. Huang, M. K. Abyaneh, M. Amati, L. Gregoratti, S. Gunther, and M. Kiskinova, *Nat. Nanotech.*, 2011, **6**, 651–657.

168. Z. Huang, Y. Lin, X. Xiang, W. Rodríguez-Córdoba, K. J. McDonald, K. S. Hagen, K.-S. Choi, B. S. Brunschwig, D. G. Musaev, C. L. Hill, D. Wang, and T. Lian, *Energy Environ. Sci.*, 2012, **5**, 8923.

169. S. R. Pendlebury, A. J. Cowan, M. Barroso, K. Sivula, J. Ye, M. Grätzel, D. R. Klug, J. Tang, and J. R. Durrant, *Energy Environ. Sci.*, 2012, **5**, 6304–6312.

170. J. B. Baxter and G. W. Guglietta, *Anal. Chem.*, 2011, **83**, 4342–4368.

171. P. U. Jepsen, D. G. Cooke, and M. Koch, *Laser Photonics Rev*, 2011, **5**, 124–166.

172. A. Paracchino, J. C. Brauer, J. E. Moser, E. Thimsen, and M. Graetzel, *J. Phys. Chem. C*, 2012, **116**, 7341–7350.

173. F. F. Abdi, T. J. Savenije, M. M. May, B. Dam, and R. Van De Krol, *J. Phys. Chem. Lett.*, 2013, **4**, 2752–2757.

174. K. R. Siefermann, C. D. Pemmaraju, S. Neppl, A. Shavorskiy, A. a. Cordones, J. Vura-Weis, D. S. Slaughter, F. P. Sturm, F. Weise, H. Bluhm, M. L. Strader, H. Cho, M. F. Lin, C. Bacellar, C. Khurmi, J. Guo, G. Coslovich, J. S. Robinson, R. a. Kaindl, R. W. Schoenlein, A. Belkacem, D. M. Neumark, S. R. Leone, D. Nordlund, H. Ogasawara, O. Krupin, J. J. Turner, W. F. Schlotter, M. R. Holmes, M. Messerschmidt, M. P. Minitti, S. Gul, J. Z. Zhang, N. Huse, D. Prendergast, and O. Gessner, *J. Phys. Chem. Lett.*, 2014, **5**, 2753–2759.

175. J. E. Katz, X. Zhang, K. Attenkofer, K. W. Chapman, C. Frandsen, P. Zarzycki, K. M. Rosso, R. W. Falcone, G. a. Waychunas, and B. Gilbert, *Science (80-.).*, 2012, **337**, 1200–1203.

176. Y. Ping, D. Rocca, and G. Galli, *Chem. Soc. Rev.*, 2013, **42**, 2437–69.

177. A. N. Andriotis and M. Menon, *J. Appl. Phys.*, 2015, **117**, 125708.

178. M. D. Bhatt and J. S. Lee, *J. Mater. Chem. A Mater. energy Sustain.*, 2015, **3**, 10632–10659.

179. A. B. Muñoz-Garcia and M. Pavone, *Phys. Chem. Chem. Phys.*, 2015, **17**, 12238–12246.

180. I. E. Castelli, D. D. Landis, K. S. Thygesen, S. Dahl, I. Chorkendorff, T. F. Jaramillo, and K. W. Jacobsen, *Energy Environ. Sci.*, 2012, **5**, 9034.

181. S. Haussener, S. Hu, C. Xiang, A. Z. Weber, and N. S. Lewis, *Energy Environ. Sci.*, 2013, **6**, 3605.

182. S. Haussener, C. Xiang, J. M. Spurgeon, S. Ardo, N. S. Lewis, and A. Z. Weber, *Energy Environ. Sci.*, 2012, **5**, 9922–9935.

183. S. Hu, C. Xiang, S. Haussener, A. D. Berger, and N. S. Lewis, *Energy Environ. Sci.*, 2013, **6**, 2984.

184. A. Berger and J. Newman, *J. Electrochem. Soc.*, 2014, **161**, E3328–E3340.

185. H. J. Lewerenz, *ECS Trans.*, 2013, **50**, 3–20.

186. K. T. Fountaine and H. a. Atwater, *Opt. Express*, 2014, **22**, A1453–A1461.

187. A. Berger, R. a. Segalman, and J. Newman, *Energy Environ. Sci.*, 2014, **7**, 1468–1476.

188. J. Hafner, C. Wolverton, and G. Ceder, *Mrs Bull.*, 2006, **31**, 659–668.

189. P. Liao and E. a. Carter, *Chem. Soc. Rev.*, 2013, 2401–2422.

190. J. Greeley, T. F. Jaramillo, J. Bonde, I. B. Chorkendorff, J. K. Norskov, and J. K. Nørskov, *Nat. Mater.*, 2006, **5**, 909–913.

191. J. K. Nørskov, T. Bligaard, J. Rossmeisl, and C. H. Christensen, *Nat. Chem.*, 2009, **1**, 37–46.

192. E. Skulason, V. Tripkovic, M. E. Bjorketun, S. Gudmundsdottir, G. Karlberg, J. Rossmeisl, T. Bligaard, H. Jonsson, and J. K. Norskov, *J. Phys. Chem. C*, 2010, **114**, 22374.

193. M. Bajdich, M. García-Mota, A. Vojvodic, J. K. Norskov, and A. T. Bell, *J. Am. Chem. Soc.*, 2013, **135**, 13521–13530.

194. E. Skúlason, G. S. Karlberg, J. Rossmeisl, T. Bligaard, J. Greeley, H. Jónsson, and J. K. Nørskov, *Phys. Chem. Chem. Phys.*, 2007, **9**, 3241–3250.

195. G. Henkelman, B. P. Uberuaga, and H. Jónsson, *J. Chem. Phys.*, 2000, **113**, 9901–9904.

196. A. Laio and M. Parrinello, *Proc. Natl. Acad. Sci. USA*, 2002, **99**, 12562–12566.

197. B. C. Wood, E. Schwegler, W. I. Choi, and T. Ogitsu, *J. Phys. Chem. C*, 2014, **118**, 1062–1070.

198. J. Oviedo, R. Sánchez-de-Armas, M. Á. S. Miguel, and J. F. Sanz, *J. Phys. Chem. C*, 2008, **112**, 17737–17740.

199. A. B. Muñoz-García and E. a Carter, *J. Am. Chem. Soc.*, 2012, **134**, 13600–3.

200. X. Shen, Y. A. Small, J. Wang, P. B. Allen, M. V. Fernández-Serra, M. S. Hybertsen, and J. T. Muckerman, *J. Phys. Chem. C*, 2010, **114**, 13695–13704.

201. Q. Guo, C. Xu, Z. Ren, W. Yang, Z. Ma, D. Dai, H. Fan, T. K. Minton, and X. Yang, *J. Am. Chem. Soc.*, 2012, **134**, 13366–13373.

202. C. Zhou, Q. Zhang, L. Chen, B. Han, G. Ni, J. Wu, D. Garg, and H. Cheng, 2010, **4**, 21405–21410.

203. U. Aschauer, Y. He, H. Cheng, S. C. Li, U. Diebold, and A. Selloni, *J. Phys. Chem. C*, 2010, **114**, 1278–1284.

204. P. T. Chen, C. L. Sun, and M. Hayashi, *J. Phys. Chem. C*, 2010, **114**, 18228–18232.

205. G. a. Kimmel, M. Baer, N. G. Petrik, J. Vandevondele, R. Rousseau, and C. J. Mundy, *J. Phys. Chem. Lett.*, 2012, **3**, 778–784.

206. P. Huang, T. A. Pham, G. Galli, and E. Schwegler, *J. Phys. Chem. C*, 2014, **118**, 8944–8951.

207. Q. Wan, L. Spanu, G. A. Galli, and F. Gygi, *J. Chem. Theory Comput.*, 2013, **9**, 4124–4130.

208. J. J. Rehr and R. C. Albers, *Rev. Mod. Phys.*, 2000, **72**, 621–654.

209. J. J. Rehr, J. J. Kas, F. D. Vila, M. P. Prange, and K. Jorissen, *Phys. Chem. Chem. Phys.*, 2010, **12**, 5503–5513.

210. J.-J. Velasco-Velez, C. H. Wu, T. A. Pascal, L. F. Wan, J. Guo, D. Prendergast, and M. Salmeron, *Science (80-.).*, 2014, **346**, 831–834.

211. D. Prendergast and G. Galli, *Phys. Rev. Lett.*, 2006, **96**, 1–4.

212. L.-M. Liu, C. Zhang, G. Thornton, and A. Michaelides, *Phys. Rev. B*, 2010, **82**, 1–4.

213. B. C. Wood, E. Schwegler, W. I. Choi, and T. Ogitsu, *J. Am. Chem. Soc.*, 2013, **135**, 15774–15783.

214. G. Tocci and A. Michaelides, *J. Phys. Chem. Lett.*, 2014, **5**, 474–480.

215. N. Kharche, M. S. Hybertsen, and J. T. Muckerman, *Phys. Chem. Chem. Phys.*, 2014, **16**, 12057–12066.

216. J. Wang, L. S. Pedroza, A. Poissier, and M. V. Fernández-Serra, *J. Phys. Chem. C*, 2012, **116**, 14382–14389.

217. M. Sumita, C. Hu, and Y. Tateyama, *J. Phys. Chem. C*, 2010, **114**, 18529–18537.

218. H. Cheng and A. Selloni, *Langmuir*, 2010, **26**, 11518–11525.

219. D. Lee, E. Schwegler, and Y. Kanai, *J. Phys. Chem. C*, 2014, **118**, 8508–8513.

220. B. C. Wood, T. Ogitsu, and E. Schwegler, *J. Photonics Energy*, 2011, **1**, 016002.

221. C. Sun, L.-M. Liu, A. Selloni, G. Q. (Max) Lu, and S. C. Smith, *J. Mater. Chem.*, 2010, **20**, 10319.

222. J. Cheng, J. Vandevondele, and M. Sprik, *J. Phys. Chem. C*, 2014, **118**, 5437–5444.

223. J. Cheng and M. Sprik, *J. Phys. Condens. Matter*, 2014, **26**, 244108.

224. J. Cheng, M. Sulpizi, J. Vandevondele, and M. Sprik, *ChemCatChem*, 2012, **4**, 636–640.

225. J. Cheng and M. Sprik, *J. Chem. Theory Comput.*, 2010, **6**, 880–889.

226. J. Tomasi, B. Mennucci, and R. Cammi, *Chem. Rev.*, 2005, **105**, 2999–3093.

227. K. Mathew, R. Sundararaman, K. Letchworth-Weaver, T. a. Arias, and R. G. Hennig, *J. Chem. Phys.*, 2014, **140**.

228. O. Andreussi, I. Dabo, and N. Marzari, *J. Chem. Phys.*, 2012, **136**.

229. C. Dupont, O. Andreussi, and N. Marzari, *J. Chem. Phys.*, 2013, **139**, 1–9.

230. M. Otani and O. Sugino, *Phys. Rev. B*, 2006, **73**, 1–11.

231. N. Bonnet, T. Morishita, O. Sugino, and M. Otani, *Phys. Rev. Lett.*, 2012, **109**, 1–5.

232. K. Letchworth-Weaver and T. a. Arias, *Phys. Rev. B*, 2012, **86**, 075140.

233. S. a Petrosyan, a a Rigos, and T. a Arias, *J. Phys. Chem. B*, 2005, **109**, 15436–15444.

234. D. Gunceler, K. Letchworth-Weaver, R. Sundararaman, K. a Schwarz, and T. a Arias, *Model. Simul. Mater. Sci. Eng.*, 2013, **21**, 074005.

235. O. Andreussi and N. Marzari, *Phys. Rev. B*, 2014, **90**, 1–16.

236. J. Cheng and M. Sprik, *Phys. Rev. B*, 2010, **82**, 081406(R).

237. J. Cheng and M. Sprik, *Phys. Chem. Chem. Phys.*, 2012, **14**, 11245–11267.

238. J. Cheng, X. Liu, J. a Kattirtzi, J. VandeVondele, and M. Sprik, *Angew. Chem. Int. Ed.*, 2014, **126**, 12242–12246.

239. U. Benedikt, W. B. Schneider, and A. a Auer, *Phys. Chem. Chem. Phys.*, 2013, **15**, 2712–2724.

240. P. Liao, M. C. Toroker, and E. A. Carter, *Nano Lett.*, 2011, **11**, 1775–1781.

241. P. Liao, E. A. Carter, P. Liao, and E. A. Carter, *J. Appl. Phys.*, 2012, **112**, 013701.

242. M. C. Toroker and E. A. Carter, *J. Phys. Chem. C*, 2012, **116**, 17403–17413.

243. M. Marsman, J. Paier, A. Stroppa, and G. Kresse, *J. Phys. Condens. Matter*, 2008, **20**, 064201.

244. V. I. Anisimov, F. Aryasetiawan, and A. I. Liechtenstein, *J. Phys. Condens. Matter*, 1997, **9**, 767–808.

245. H. J. Kulik, M. Cococcioni, D. A. Scherlis, and N. Marzari, *Phys. Rev. Lett.*, 2006, **97**, 103001.

246. N. J. Mosey and E. A. Carter, *Phys. Rev. B*, 2007, **76**, 155123.

247. N. J. Mosey, P. Liao, and E. A. Carter, *J. Chem. Phys.*, 2008, **129**, 014103.

248. J. H. Skone, M. Govoni, and G. Galli, *Phys. Rev. B*, 2014, **89**, 195112.

249. V. Stevanovic, S. Lany, D. S. Ginley, W. Tumas, and A. Zunger, *Phys. Chem. Chem. Phys.*, 2014, **16**, 3706–3714.

250. R. J. Bartlett and M. Musiał, *Rev. Mod. Phys.*, 2007, **79**, 291–352.

251. R. J. Bartlett and J. F. Stanton, in *Rev. Comput. Chem.*, eds. K. B. Lipkowitz and D. B. Boyd, VCH Publishers, New York, 1994, vol. 5, pp. 65–169.

252. W. M. C. Foulkes, L. Mitas, R. J. Needs, and G. Rajagopal, *Rev. Mod. Phys.*, 2001, **73**, 33–83.

253. C. Adamo and D. Jacquemin, *Chem. Soc. Rev.*, 2013, **42**, 845–856.

254. M. a L. Marques and E. K. U. Gross, *Annu. Rev. Phys. Chem.*, 2004, **55**, 427–455.

255. S. Botti, A. Schindlmayr, R. Del Sole, and L. Reining, *Reports Prog. Phys.*, 2007, **70**, 357–407.

256. M. K. Nazeeruddin, F. De Angelis, S. Fantacci, A. Selloni, G. Viscardi, P. Liska, S. Ito, B. Takeru, and M. Grätzel, *J. Am. Chem. Soc.*, 2005, **127**, 16835–16847.

257. F. De Angelis, S. Fantacci, and A. Selloni, *Nanotechnology*, 2008, **19**, 424002.

258. A. V Akimov, A. J. Neukirch, and O. V Prezhdo, *Chem. Rev.*, 2013, **113**, 4496–4565.

259. G. Onida, L. Reining, and A. Rubio, *Rev. Mod. Phys.*, 2002, **74**, 601–659.

260. M. S. Hybertsen and S. G. Louie, *Phys. Rev. B*, 1986, **34**, 5390–5413.

261. M. Rohlfing and S. G. Louie, *Phys. Rev. B*, 2000, **62**, 4927–4944.

262. H.-V. Nguyen, T. A. Pham, D. Rocca, and G. Galli, *Phys. Rev. B*, 2012, **85**, 081101.

263. T. A. Pham, H.-V. Nguyen, D. Rocca, and G. Galli, *Phys. Rev. B*, 2013, **87**, 155148.

264. M. Govoni and G. Galli, *J. Chem. Theory Comput.*, 2015, 150112171036002.

265. D. Opalka, T. A. Pham, M. Sprik, and G. Galli, *J. Chem. Phys.*, 2014, **141**.

266. T. A. Pham, D. Lee, E. Schwegler, and G. Galli, *J. Am. Chem. Soc.*, 2014, **136**, 17071–17077.

267. T. A. Pham, C. Zhang, E. Schwegler, and G. Galli, *Phys. Rev. B*, 2014, **89**, 060202.

268. N. Kharche, J. T. Muckerman, and M. S. Hybertsen, *Phys. Rev. Lett.*, 2014, **113**, 1–6.

269. C. Zhang, T. A. Pham, F. Gygi, G. Galli, C. Zhang, A. Pham, F. Gygi, and G. Galli, *J. Chem. Phys.*, 2013, **138**, 2011–2015.

270. R. J. Bartlett, *Annu. Rev. Phys. Chem.*, 1981, **32**, 359–401.

271. G. D. I. Purvis and R. J. Bartlett, *J. Chem. Phys.*, 1982, **76**, 1910–1918.

272. I. Shavitt, in *Methods of Electronic Structure Theory*, ed. H. F. I. Schaefer, Plenum Press, New York, Vol. 3., 1977, pp. 189–275.

273. B. O. Roos, P. R. Taylor, and P. E. M. Siegbahn, *Chem. Phys.*, 1980, **48**, 157–173.

274. K. Andemson, P. Malmqvist, B. Roos, A. J. Sadlej, and K. Wolinskit, *J. Phys. Chem.*, 1990, **94**, 5483–5488.

275. Y. Yang, M. A. Ratner, and G. C. Schatz, *J. Phys. Chem. C*, 2013, **117**, 21706–21717.

276. Y. Yang, M. A. Ratner, and G. C. Schatz, *J. Phys. Chem. C*, 2014, **118**, 29196–19208.

277. P. Huang and E. A. Carter, *Annu. Rev. Phys. Chem.*, 2008, **59**, 261–290.

278. P. Liao and E. A. Carter, *J. Phys. Chem. C*, 2011, **115**, 20795–20805.

279. C. F. Craig, W. R. Duncan, and O. V. Prezhdo, *Phys. Rev. Lett.*, 2005, **95**, 1–4.

280. C. M. Isborn and X. Li, *J. Chem. Theory Comput.*, 2009, **5**, 2415–2419.

281. E. Tapavicza, I. Tavernelli, and U. Rothlisberger, *Phys. Rev. Lett.*, 2007, **98**, 1–4.

282. A. V. Akimov, J. T. Muckerman, and O. V. Prezhdo, *J. Am. Chem. Soc.*, 2013, **135**, 8682–8691.

283. A. C. T. van Duin, S. Dasgupta, F. Lorant, and W. A. Goddard, *J. Phys. Chem. A*, 2001, **105**, 9396–9409.

284. D. Raymand, A. C. T. Van Duin, W. a. Goddard, K. Hermansson, and D. Spångberg, *J. Phys. Chem. C*, 2011, **115**, 8573–8579.

285. M. Raju, S. Y. Kim, A. C. T. Van Duin, and K. a. Fichthorn, *J. Phys. Chem. C*, 2013, **117**, 10558–10572.

286. S. Y. Kim, N. Kumar, P. Persson, J. Sofo, A. C. T. Van Duin, and J. D. Kubicki, *Langmuir*, 2013, **29**, 7838–7846.

287. S. Kerisit and K. M. Rosso, *J. Chem. Phys.*, 2007, **127**, 124706.

288. S. K. Wallace and K. P. McKenna, *Adv. Mater. Interfaces*, 2014, n/a–n/a.

289. E. Santos, A. Lundin, K. Pötting, P. Quaino, and W. Schmickler, *Phys. Rev. B*, 2009, **79**, 235436.

290. W. I. Choi, B. C. Wood, E. Schwegler, and T. Ogitsu, *J. Phys. Chem. C*, 2013, **117**, 21772–21777.

291. B. C. Wood, T. Ogitsu, and E. Schwegler, *J. Chem. Phys.*, 2012, **136**.

292. C. Wolverton and A. Zunger, *Phys. Rev. Lett*, 1998, **81**, 606–609.

293. S. Curtarolo, G. L. W. Hart, M. B. Nardelli, N. Mingo, S. Sanvito, and O. Levy, *Nat. Mater.*, 2013, **12**, 191–201.

294. M. Ferhat and F. Bechstedt, *Phys Rev. B*, 2002, **65**, 1–7.

295. J. C. Thomas, J. M. Millunchick, N. a. Modine, and A. Van Der Ven, *Phys. Rev. B*, 2009, **80**, 1–12.

296. R. Osorio, J. E. Bernard, S. Froyen, and A. Zunger, 1992, **45**.

297. C. Ludwig, T. Gruhn, C. Felser, and J. Windeln, *Phys. Rev. B*, 2011, **83**, 1–8.

298. Z. B. Chen, T. F. Jaramillo, T. G. Deutsch, A. Kleiman-Shwarsctein, A. J. Forman, N. Gaillard, R. Garland, K. Takanabe, C. Heske, M. Sunkara, E. W. McFarland, K. Domen, E. L. Miller, J. A. Turner, and H. N. Dinh, *J. Mater. Res.*, 2010, **25**, 3–16.

299. H. N. Dinh and Z. B. Chen, *Photoelectrochemical Water Splitting Standards, Experimental Methods, and Protocols*, Springer, New York, 2013.

300. C. Kranz, *Analyst*, 2014, **139**, 336–352.

301. J. V. Macpherson and P. R. Unwin, *Anal. Chem.*, 2001, **73**, 550–557.

302. G. Shi, L. F. Garfias-Mesias, and W. H. Smyrl, *J. Electrochem. Soc.*, 1998, **145**, 2011–2016.

303. Y. Zhang, H. Li, L. Wang, H. Wang, X. Xie, S.-L. Zhang, R. Liu, and Z.-J. Qiu, *Sci. Rep.*, 2015, **5**, 7938.

304. Y. Lee and A. J. Bard, *Anal. Chem.*, 2002, **74**, 3626–3633.

305. Y. Lee, Z. Ding, and A. J. Bard, *Anal. Chem.*, 2002, **74**, 3634–3643.

306. T. H. Treutler and G. Wittstock, *Electrochim. Acta*, 2003, **48**, 2923–2932.

307. F. Guillaume, J. Evju, T. L. Knutson, and W. H. Smyrl, *J. Electrochem. Soc.*, 2003, **150**, B262–B265.

308. W.-J. Lee, F. Guillaume, T. L. Knutson, and W. H. Smyrl, *J. Electrochem. Soc.*, 2005, **152**, B111–B115.

309. K. F. Domke and B. Pettinger, *ChemPhysChem*, 2010, **11**, 1365–1373.

310. M. D. Sonntag, E. A. Pozzi, N. Jiang, M. C. Hersam, and R. P. Van Duyne, *J. Phys. Chem. Lett.*, 2014.